MISS ARIADNA COPPA VIGLIOCCO (Orcid ID : 0000-0003-0466-5133)

Article type : Original Article

Atypical ooid diversity in the Upper Cretaceous Yacoraite Formation, Argentina

Ariadna Coppa Vigliocco[*1, 2], *Ricardo A. Astini*[1, 2], *Fernando J. Gomez*[1, 2]

1. Centro de Investigaciones en Ciencias de la Tierra (CICTERRA). Consejo Nacional de Investigaciones Científicas y Técnicas (CONICET), Haya de la Torre s/n, Córdoba, Argentina.
2. Universidad Nacional de Córdoba (UNC-FCEFyN)

E-mail addresses: *ariadna.coppa@mi.unc.edu.ar (A. Coppa Vigliocco), ricardo.astini@unc.edu.ar (R. A. Astini), fjgomez@unc.edu.ar (F. J. Gomez)

ABSTRACT

This study reports on ooid diversity from different lithotypes of the Yacoraite Formation (Salta Group basin) in the Central Andes of north-west Argentina. The ooids display a variety of internal and external morphologies that may be deployed as proxies for seawater chemistry and hydrodynamic processes. A short review of nomenclature problems is first discussed, followed by presentation of a two-fold quantitative and qualitative methodology. Our proposed classification addresses internal and external ooid characters in order to understand growth in response to various environmental processes at an individual particle level. This classification allows discrimination between a variety of morphologies, but also evaluation of the complexity of the processes involved in ooid formation as seen in the fossil record. This study evaluates whether the ooids present within the Yacoraite Formation share similarities with ooids formed in marine versus marine lagoon and/or lacustrine environments. A possible lacustrine interpretation finds

This article has been accepted for publication and undergone full peer review but has not been through the copyediting, typesetting, pagination and proofreading process, which may lead to differences between this version and the Version of Record. Please cite this article as doi: 10.1111/SED.13007

its origin in the diverse assemblage of ooid morphotypes present, which exceeds the variations described for marine ooids. However, growth paths and occurrence of various compound morphologies point to intense marine recycling, suggesting little accommodation. Together with other sedimentological characteristics, for example, bi-directional cross-bedding, tidal shoals, hummocky cross-stratification and exposure surfaces, these features suggest that marine processes had an impact on the sediments. Therefore, the ooid assemblage of the Cretaceous Yacoraite Formation was most likely formed in a shallow coastal lagoon in the framework of an epicontinental sea that at times experienced marine flooding events. A detailed evaluation of processes involved in oolite formation is needed in order to improve the stratigraphic and palaeoenvironmental understanding of ooid formation through time. This includes examining alternating constructive and destructive stages, early binding and cementation, reworking, recycling and averaging processes.

KEYWORDS: Cretaceous, epicontinental carbonates, ooid diversity, ooid growth, quantitative analysis, Yacoraite Formation.

INTRODUCTION

Ooids consist of largely sand-sized spherical to subspherical carbonate particles, generally up to about 2 mm in diameter, with concentric calcareous layers growing around a nucleus of variable origin and composition (Flügel, 1982; Tucker & Wright, 1990). Ooid grains form rocks called oolites (Brückmann, 1721; Burne *et al.,* 2012), which may comprise ooids exhibiting a variety of textures. Carbonate ooids are typically formed in carbonate saturated and agitated shallow waters, thus promoting precipitation as spherical particles (Bathurst, 1972; Folk & Linch, 2001; Trower *et al.,* 2017, 2018). Ooid grains are represented in all geological periods (Kalkowsky, 1908; Paul *et al.,* 2011, Siahi *et al.,* 2017) from the present to the deep past. Their size varies from <1 mm to >2 mm, as shown by the giant ooids of Neoproterozoic platforms (Sumner & Grotzinger, 1993; Trower & Grotzinger, 2010; Trower, 2020) or those of the end-Permian in South China (Li *et al.,* 2013, 2015; Lehrmann *et al.,* 2012; Mei & Gao, 2012; Li *et al.,* 2020). Their geological interest stems from the fact that ooids provide valuable information on current–sediment interactions and aqueous carbonate chemistry (Deelman, 1978; Rankey &

Reeder, 2012). In addition, ooids can reflect a biosignature if formed via microbial mediated precipitation (Ariztegui *et al.,* 2012; Diaz *et al.,* 2017; Harris *et al.,* 2019). Oolites are significant in the evolution of marine and lacustrine carbonate stratigraphic records of all ages worldwide, and frequently can be linked to hydrocarbon accumulations (Sandberg, 1975; Ferguson & Ibe, 1982; Davaud & Girardclos, 2001; Rankey *et al.,* 2018).

Recently, several contributions have provided new insights into the origin of ooids based on their detailed internal and external aspects (see Diaz & Eberli, 2019, and references therein). Some studies have proposed adding new genetic terminology (*mature* versus *immature ooids*, Sipos *et al.,* 2018) and others (Batchelor *et al.,* 2018) have shown problems arising through early diagenesis, which should be taken in consideration and may complicate interpretations. An up-to-date synthesis of the existing morphological and textural varieties is here needed in order to: (i) clarify the terminology; and (ii) initiate the debate on possible origins of a wide range of morphologies.

An all-encompassing descriptive framework may help with the depositional environmental interpretation of ancient studies. Understanding the balance between growth and abrasion and their impact on the size of these particles (Strasser, 1986; Sumner & Grotzinger, 1993; Sipos *et al.,* 2018) has been revitalized in recent experimental research (Trower *et al.,* 2017, 2018, 2020). However, the variety of features present and the controls determining their formation are still a matter for discussion and a range of possibilities are proposed ranging from dominant physical–chemical processes (Deelman, 1978; Sumner & Grotzinger, 1993; Brehm *et al.,* 2006; Anderson *et al*., 2020) to dominant biogenic processes (Ariztegui *et al.,* 2012; Edgcomb *et al.,* 2013; Li *et al.,* 2015, 2019; Batchelor *et al.,* 2018; Sipos *et al.,* 2018; Diaz *et al.,* 2017, Harris *et al.,* 2019).

The aim of this contribution is to document diverse morphological attributes of ooids present in the carbonate intervals of the Yacoraite Formation, a Late Cretaceous–Palaeocene unit in north-west Argentina. The study focusses on: (i) quantitative considerations relating to size, sorting and morphology; and (ii) qualitative aspects of the internal fabric of the ooids. A set of procedures and criteria are proposed that allow interpretation of the processes involved in ooid formation, and consolidation of a common terminology that can be applied throughout the stratigraphic record, regardless of the

age. An alternation of lacustrine and marine deposits is proposed to explain growth trajectories that may be present in coastal settings, including tidal flats and coastal lagoons, where both constructive and destructive processes of the ooid laminae as well as ooid aggregation occur.

OOID TERMINOLOGY

The number of individual grains serving as an ooid nucleus, as well as their nature and shape, can be taken into account in order to differentiate between ***simple*** and ***compound*** ooids (Fig. 1) following Flügel (1982). According to this, simple ooids are grains with one particle in their interior, whereas compound ooids consist of two or more particles bound together to form the nucleus of a new ooid. Other names that have been used as synonyms for compound ooids are composite or complex ooids (Carozzi, 1964; Poncet, 1984) and poly-ooids (Kalkowsky, 1908; Chatalov, 2005).

Another common criterion considers the relative position of the nucleus to discern whether the layers develop centred or eccentrically around the nucleus (Fig. 1). When the nucleus is off-centre within the ooid, it is classified as ***eccentric***. (Gasiewics, 1984; Flügel, 2004).

The cortex of ooids may include one or several envelopes. When finer divisions can be detected, it may be important to differentiate laminae as an internal attribute of the linings. A lamina has an average thickness of 1 to 3 microns, but cortical layers can be up to a millimetre in thickness (Flügel, 2004). Ooids with a single cortical layer (Bathurst, 1967) are defined as ***superficial ooids*** (Carozzi, 1957). According to Flügel (2004), the thickness of the layer should be at least half the diameter of the complete ooid. On the other hand, ***multiple-layered ooids*** are characterized by two or more laminae visible at microscopic scale (Fig. 1). In the literature, these ooids are classified as normal ooids (Flügel, 2004; Sandberg, 1975; Heller *et al.,* 1980) or regular ooids (Li *et al.,* 2015).

Various other features may also occur within the cortex package of multilayered ooids that can be used to unravel the ooid cortical stratigraphy (Trower *et al.,* 2020). The thickness trends of the laminae (Batchelor *et al.,* 2018; Sipos *et al.,* 2018) represent the accretion history (for example, thickening or thinning or random distribution, Fig. 1), as long as there is some certainty that the thin section traversed the ooid centre (visible nucleus). The individual laminae may display the same thickness around the entire ooid,

implying consistency of shape (Sandberg, 1975). However, ooids usually show shape modifications because their laminae thickness is not constant, with thickness compensations or erosion surfaces expressed as unconformities (Sipos *et al.,* 2018; Trower *et al.,* 2020). Some ooids may show internal angular unconformities, whereas some others demonstrate subtle internal truncations. Within oolitic limestones, partially decoupled laminae may occur that remain unbound, and broken pieces may develop layers around them; these particles have been referred to as ***regenerated*** (after ***broken***) ooids by Carozzi (1961). Berg (1944) referred to them as 'hiatus ooids'.

In relation to laminae microfabrics, the fibrous–radial cortex displays crystals that grow perpendicular to the surface of the laminae ('beta ooids' of Purser, 1980), and tangential to those crystals whose major axes are aligned to the surface of the laminae ('alpha ooids' of Purser, 1980). Variable degrees of micritization and recrystallization may exist, affecting the nuclei or individual laminae. Ooids with micritic laminae are not differentiated because their composition varies between amorphous or cryptocrystalline components at the microscopic scale. When an ooid has a completely micritic appearance and has lost its primary rounded shape and internal laminae, it falls outside the classification scheme and is regarded as another category of allochemical particle, namely a peloid.

Regarding the shape, in addition to the classical external rounded shapes (spheroid and ellipsoid), a variety of other shapes can be present (for example, rod-like or banana-like). In the classification scheme (Fig. 1), a morphological term is included describing the external surface of the ooid. For this, the terms ***smooth***, ***crenulate*** (micro-rugged), ***festoon*** (lobate) and ***irregular*** or amebiform (embayed or swalen) are used, sometimes showing a range between them. As the surface becomes more complex, it acquires different names: Cerebroid ooids (Carozzi, 1962) are considered a special case of festoon morphologies. However, the term emphasizes the internal morphology, characterized by an irregular contorted pattern (Batchelor *et al.,* 2018). Alternatively, this mottled pattern can be described as zebra-like, and this study considers it as an internal recrystallization feature and retains the term festoon for the external structure. Lobate forms consist of constant wavelength, convex, juxtaposed segments that may be separated by shorter concave segments (Sandberg, 1975). This external lobate shape coincides with fan-shaped crystal bundles ('rays' of Eardley 1938; Kahle, 1974) or sets of

fibro-radiated or bladed crystals (with frequent fascicular optic extinction), alternating with micritic dark areas. More recently, Batchelor *et al.* (2018) included similar lobate shapes within diagenetic modifications of ideal oolite structures, and proposed the use of two different names originally coined by Kalkoswky (1908), s*pindeltruktur* and *kegelstruktur*. It is clear that detailed descriptions (e.g. Sandberg, 1975) help to support the diagenetic, chemical or biological interpretations of the ooids.

GEOLOGICAL SETTING AND STRATIGRAPHY

During the Cretaceous, north-west Argentina (Fig. 2A) was affected by extensional processes that resulted in the development of retro-arc rift basins that were filled with as much as 5000 m thick series of the Salta Group. The latter is dominated by sedimentary and a few interbedded magmatic rocks (Moreno, 1970; Salfity & Marquillas, 1994; Galliski & Viramonte, 1988; Marquillas *et al.,* 2005; Hernández *et al.,* 1999, 2008). The basin presents a 'Y' shape distribution on the geological map (Fig. 2B), in which the north-western branch is represented by the Tres Cruces sub-basin, directly connected with Bolivia and the study site (Tasistro-Hart *et al.,* 2020). The north-eastern branch corresponds to the Lomas de Olmedo sub-basin that has important hydrocarbon reserves. The southern branch encloses the Metán–Alemania depocentre, and represents the southernmost termination of a retro-Andean rift zone (Salfity & Marquillas, 1994; Grosso *et al.,* 2013; Gomes *et al.,* 2020).

The basin infill displays an initial syn-rift stage with intrabasinal volcanism and coarse-grained clastics localized within grabens and half-grabens (Salfity & Marquillas, 1994). Onlapping towards the basin edges and intervening topographic highs is a Late Campanian to Early Palaeocene carbonate interval, which has a great regional extent and is interpreted as a sag-stage fill (Stark, 2011). In Argentina these limestones are known as the Yacoraite Formation (Turner, 1959; Moreno, 1970). They have been correlated with the El Molino Formation in Bolivia (Sempere, 1995; Sempere *et al.,* 1997), and their deposition occurs between *ca* 73 Ma and 64 Ma (Maastrichtian–Danian) (Rouchy *et al.,* 1993, Sempere *et al.,* 1997, Marquillas *et al.,* 2007, 2011; Tasistro-Hart *et al.,* 2020). Also in Bolivia, similar deposits have been interpreted as either shallow marine (e.g. Marquillas *et al.,* 2005) or lacustrine deposits (e.g. Guimarães, 2014; Gomes *et al*., 2020). This broad range of settings is substantiated by the mixture of marine and

continental biotas exhibited, including marine fish and benthic foraminifera but also dinosaur tracks (Benedetto & Sánchez, 1972; Gayet *et al.,* 1993; Sempere *et al.,* 1997; Console Gonella *et al.,* 2017). The interpretation of marine and continental facies alternations has fostered a long-lasting discussion in relation to the overall cause of the variation in shallow-marine to continental lacustrine depositional conditions. Tasistro-Hart *et al.* (2020) recently suggested that the marine incursions relate to obliquity steered astronomical cycles, because of the presence of sedimentary periodicities between short eccentricity, precession and semi-precession in the El Molino Formation, along the Bolivian Cordillera Oriental. Although the interpretation of the palaeogeographic connections is still controversial, it is suggested that marine transgressions reached as far south as north-west Argentina, and induced the deposition of at least the marine part of the Yacoraite limestones (Macellari, 1988; Sempere *et al.,* 2004; Marquillas *et al.,* 2005; Console-Gonella *et al.,* 2017).

In this study, the Yacoraite Formation was examined in sections along the Espinazo del Diablo range (Figs 2C and 3) in the Argentine Cordillera Oriental (Jujuy Province), which is part of the Tres Cruces sub-basin (Moreno, 1970). Access to the region is through a 25 km dirt-road west from Humahuaca town. In this section, >1000 m of Cretaceous synrift deposits are superbly exposed and display laterally continuous limestones of the Yacoraite Formation that overlie aeolian deposits of the Lecho Formation (Fig. 4A). The sediments of the Yacoraite Formation are covered by lacustrine red beds of the Maíz Gordo Formation (Fig. 4B). At this outcrop, three distinct informal members are defined within the Yacoraite Formation (Fig. 3A): (i) a lower *ca* 113 m interval of yellowish to greyish oolitic sandy carbonates interbedded with stromatolitic limestone, alternating with minor shale partings and tuffs (Fig. 3B); (ii) an intermediate interval composed of greenish to purplish shale-rich sediments (*ca* 65 m) with few interbedded limestones; and (iii) an upper interval (*ca* 137 m) characterized by brownish marl-rich layers, interbedded with ostracod–gastropod-rich limestones and distinct metre-scale tabular stromatolite beds at the top. This study focusses on the ooid-rich limestones of the lower interval (Fig. 3B).

METHODS

The stratigraphic sequences were described bed-by-bed at the centimetre scale in order to determine bed thickness, surface features, sedimentary structures, fossils and lithological classification (Dunham, 1962). The sections were photographed and sampled for lithotype characterization. Thin sections were prepared by conventional methods for analysis by transmitted-light microscopy. The thin sections were stained with Alkaline Alizarin Red S to differentiate between calcite and dolomite. In addition, polished sections of hand samples were used to describe large-scale sedimentary features.

An integrated analysis was applied to the study of the ooids associated with different lithotypes recognized in this interval, concentrating on oolitic grainstones and a variety of rudstones. These layers were especially selected because they contain high percentages of ooids, with a diversity in sizes and shapes. This procedure integrates: (i) the analysis of the quantitative aspects in relation to size, sorting and morphology; and (ii) the documentation of the qualitative aspects of the internal fabric of the ooids.

Quantitative shape parameters

Fiji software (Rasband, 2004, Schindelin *et al.,* 2012) was chosen to measure quantitative parameters (see Table 1) like imaging, tracing and determination of statistical parameters of shape, aspect ratio, circularity and roundness. For more details about methods see the supporting online material (Section S1).

Several traverses were made for each thin section and a total of 400 to 500 points per section were counted to obtain sufficiently accurate percentages of ooid types. Shape parameters, determined by image analysis, are limited to the two dimensions that are the projection of the particle on the plane. Fiji includes a set of measurements including shape descriptors, which was used in the present analysis because this may have implications for the mode of transport and deposition of the ooids studied (Folk & Ward*,* 1957; Cox & Budhu, 2008; Pruss & Clemente*,* 2011; Heilbronner *et al.,* 2014; Trower *et al.,* 2018). Shape descriptors included in this analysis, in addition to the Feret diameter (taken as the distance between the two furthest points on the particle, independent of its shape), include: (i) the aspect ratio (AR), being the dimensions of the long and short axis of the grain, varying from one to infinite, as a measure of particle elongation; (ii) circularity, calculated as $4\pi A/P^2$*,* where P is the perimeter and A is the area of the particle projection; a perfect circle has a circularity of one and is defined as the degree to

which the particle is similar to a circle; and (iii) roundness, calculated as $4A/\pi LM^2$, where *LM* is the long-axis of an ellipse that can fit an object, which is a measure of the sharpness of the corners of a grain and is expressed as a ratio to the average curvature of the particle as a whole, independent of the shape (Krumbein, 1941; Riley, 1941; Barrett, 1980; Blott & Pye, 2008; Cox & Budhu, 2008; Sochan *et al.,* 2015). To extend and complement the individual ooid analysis the cortex thickness in millimetres, number of laminae and nuclei diameter were also added.

The quantitative analysis also included the population parameter as the median grain size (D_{50}) and degree of sorting. A series of statistical measurements were performed that included: (i) central tendency (median, mode and mean); and (ii) the degree of sorting, kurtosis and skewness that emphasized the shape distribution (Friedman, 1961; Folk, 1974). Statistical parameters and graphic representations of the grain-size are given in phi units according to the formula: $\Phi = -\log_2 d$, where *d* is the external ooid diameter in millimetres (Folk & Ward, 1957).

Qualitative ooid characterization

A series of analytical steps (see flow diagram in Fig. 6) were developed to determine the different qualitative aspects shown by the ooids for the diverse lithotypes, and included both the nucleus and the cortex (Fig. 1). First, whether a nucleus could be identified was determined. When present, the nature or composition (carbonate versus non-carbonate), its size, shape, preservation and roundness were determined. A comparison of nuclei material with other allochems (for example, bioclasts and intraclasts) or non-allochemical grains (extraclasts) in the sample, was included in the description.

Following identification (Fig. 6), information on the laminae microfabrics, was determined. This included the orientation of the crystals (fibrous radial, concentric tangential, radial and concentric, micritic or a combination of these types) within the cortex.

LITHOTYPES, ENVIRONMENTS AND OOID DIVERSITY

In this section the main lithotypes including ooid diversity are described. Stromatolite lithotypes, both planar-crenulate within the tidally influenced shallow-water environments

and domal isolated or laterally-linked largely subtidal deposits, also include very thin ooid-rich laminae that alternate with clotted peloidal or crystalline fabrics.

Thin-bedded wavy peloidal–oolitic grainstone

This lithotype occurs in the lower part of the stratigraphic succession (Fig. 3B) and consists of fine-grained to moderately sorted (1–2 cm and up to 10 cm thick) amalgamated sandy limestones. (Fig. 5A). The sediments show platy to wavy bedding with parallel to undulating upper and lower contacts and minor (millimetre-scale) finer-grained muddy partitions. They also contain bimodal trough cross-lamination showing bundles of oppositely inclined laminae with frequent scooped surfaces and internal truncations. Largely symmetrical ripple forms occur (ripple indexes ranging between 10 : 1–6 : 1) with strongly symmetrical chevron shapes to slightly asymmetrical forms (symmetry indexes <2). Plan forms show sharp, straight to slightly sinuous ripple crests that yield remarkable continuity and constant separation with occasional bifurcations, zigzag crests and rare interference tile-like patterns. This lithotype shows subtle bioturbation.

Composition: Allochems are represented by ooids (*ca* 40%), detrital grains (*ca* 18%), peloids (*ca* 15%), bivalves and ostracods (<2%) and rounded intraclasts (<5%). Peloids are rounded and slightly smaller than ooids on average. Sparry calcite (*ca* 20%) cements and local micrite (mudstones) partitions are present.

Environmental interpretation: Thoroughly laminated and thinly bedded wavy peloidal–oolitic grainstones are interpreted as a relatively high-energy shallow subtidal lithotype. Pervasive bimodal cross-lamination (chevron-like) showing bundles of oppositely inclined laminae with frequent scooped surfaces and internal truncations, together with plan form symmetrical ripple marks, indicate predominant oscillatory flow activity under the influence of fair-weather wave base. Tile-like patterns as well as zigzag crests are interpreted as wave ripple defects due to changing flow disequilibrium and perturbation components associated with near-circular elliptical forcing at the top of the bottom boundary layer (Roos & Blondeaux, 2001, Perron *et al*., 2018, Myrow *et al*., 2018). No evidence of subaerial exposure was found. Recurrent amalgamation and a very high sands/fines ratio indicate deposition within a high-energy predominantly grainy sublittoral (subtidal) facies belt.

Ooid diversity: This lithotype shows the best ooid sorting and the frequency histogram has a near-symmetrical size distribution (Table 1; Fig. 7A). Simple multiple-layered ooids dominate (Table 2; Fig. 8A to C), usually consisting of two or three laminae. They display radial calcite crystals with a concentric arrangement of envelopes, alternating with thin dark micritic layers. Rounded ooids predominantly have detrital nuclei (99% quartz). Centred nuclei form the bulk of the ooids, although eccentric types also occur. Superficial ooids are also present and consist of radially oriented acicular calcite crystals within the cortex, noting some laminae are formed by homogeneous, cloudy and dense micrite (Table 2). The superficial lining is sometimes incomplete and uneven (often thicker on one side of the nucleus than on the other) and the external surface of all ooid types in this lithotype is smooth (Fig. 8A). Ooids with a broken and decoupled external cortical layer are also present. Subordinately, cortex fragments occur that were later laminated with one or two layers of calcite with a fibrous–radial fabric. In general, the ooids show line contacts and slight interpenetrations (Fig. 8B).

Oversized compound ooids (Table 2) generally contain two individuals with an elongate and irregular shape. They also can include simple-ooids, quartz grains, micrite peloids and bioclasts, which show point grain-contacts or are cushioned by a variable amount of micrite. Compound ooids usually develop a superficial rim *ca* 0.02 mm thick of calcite fibrous–radial fabric that completely envelops the ooid. In some cases, the envelope is made of micrite (Fig. 8C).

Graded skeletal–oolitic grainstone–packstone

This lithotype occurs in the lower and upper part of the sequence (Fig. 3B), and is characterized by grey and yellowish tabular limestones with a flat to wavy base and top. Bed thickness varies between 5 cm and 10 cm, including large skeletal remains (Fig. 5B). The tabular beds are continuous throughout the outcrop with little thinning over hundreds of metres. They are interbedded with thin-bedded wavy peloidal–oolitic grainstone (see *Thin-bedded wavy peloidal–oolitic grainstone* section). Occasionally, these levels show sets of cross-laminae and frequent symmetrical ripples are common at the top. Sparse rip-up clasts and flat-pebble intraclasts occur throughout (seldom imbricated). Internally, the beds exhibit parallel lamination, hummocky and swaley cross-stratification (wavelengths between tens of centimetres and 1 m) and several low-angle truncations

(<10°). Bioclasts are prominent in these lithologies and can be easily differentiated from other allochems.

Composition: This lithotype is composed of *ca* 50% ooids and *ca* 30% bioclasts, including outsized complete molluscs (bivalve and gastropod) to fragmented shell hash, sometimes nested and visibly distorted by bioturbation (Fig. 5B). Subordinate foraminifera and charophyte remains are present as well as intraclasts (*ca* 5%, usually fragments of oolite-rich grainstones–packstones or mudstones either clotted–laminated or massive) and up to *ca* 10% detrital grains. Sparry calcite cement is pervasive (13% in average) and partial intergranular to intragranular dolomitization is present. Silt-sized interstitial sediment is deposited on free surfaces, frequently on larger bivalve shells (Fig. 8E).

Environmental interpretation: Graded skeletal–oolitic grainstone–packstones are interpreted to represent decelerating bioclastic-rich storm beds that accumulated between fair-weather wave base and storm-wave base (Ginsburg & Hardie, 1975; Kidwell *et al.,* 1986; Gomez & Astini, 2015). Their composition diversity (Benedetto & Sanchez, 1972; Marquillas *et al.,* 2005, 2007; Console Gonella *et al.,* 2012, 2017) indicates various relatively proximal sources within a shallow marine setting.

Ooid diversity: The ooids in this lithotype have rounded to banana-like and rod-like shapes with sizes that vary between medium to coarse-sand. Elongated shaped ooids predominate and bioclasts are included mainly as nuclei, although they are also common in the framework of this lithotype. Histograms show positively skewed asymmetrical distribution (Fig. 7B) and moderately to well-sorted ooids (Table 1).

Multiple-layered ooids dominate, over 80%, with clearly identifiable nuclei largely composed of ostracods, gastropods, bivalve fragments and peloids (Table 2). A smaller amount of detrital extraclasts is found both in the simple ooid nuclei and in the sediment matrix (Fig. 8D). As more rounded types show an even cortex thickness, elongated (rod-like) types show differential thickening towards the larger apparent diameter (Fig. 8D and E). When nuclei consist of concave bioclasts, the curvature is compensated for after a few layers by subtle envelope thickening within the concave side.

This lithotype does not include simple superficial-ooids but contains various skeletal grains with micrite linings (Table 2). Ostracods generally preserve both shells that may be substantially thickened, sometimes making it difficult to distinguish between

ooids and bioclasts. Simple multilayered ooids include between two and ten layers, where light-brown fibrous–radial or radial–concentric fabric alternates with thin dark micritic laminae. Some ooids start with an initial dark micritic lamina that completely surrounds a bioclastic nucleus followed by a light fibrous–radial lamina. Ooids with smooth external surfaces predominate over those with irregular surfaces. In some ooids, especially the larger ones, the last laminae may be detached from the others, although they only reach 5% of the total ooids.

Graded intraclastic oolitic grainstone–rudstone

This lithotype occurs in the lower and middle part of the succession, although it is less frequent in the upper part of the sequence (Fig. 3B). The sediments consist of grey-yellowish medium to very coarse-sand and granule size, thin to medium-bedded tabular limestones, strongly graded and yielding pebble to cobble intraclastic lags at the base (Fig. 5C). Intervals can be traced across tens of metres along the outcrops. The basal boundaries are sharp and erosive; tops are more gradual with symmetrical ripples overlain by thin mud drapes. Barely observable parallel lamination, subtle hummocky-cross stratification (HCS) and rare low-angle truncations (<10°) are also present within these beds. Texturally they vary from grainstones (packstones) to rudstones (floatstones). Beds normally grade from clast-supported (centimetre-scale) coarser lags (rudstones) to coarse-medium-size oolite grainstones, sometimes yielding very coarse-grained tails. This facies as well as *graded skeletal–oolitic grainstone–packstone* are interbedded with *thin-bedded wavy peloidal–oolitic grainstone* layers that occur isolated or amalgamated forming packages of as much as two or three beds (*ca* 50 cm thick).

Composition: The sediments comprise *ca* 65% ooids and *ca* 35% intraclasts with rare detrital grains (<1%), largely quartz. Intraclasts are poorly-sorted and compositionally range from grainstones to mudstones, and at times display a slightly more yellowish colour and partial dolomitization (inset Fig. 5C). Intraclasts include rounded–subrounded to angular–subangular (Fig. 8H) pebbles and cobbles (<64 mm) of oolite-rich grainstones and packstones, and up to decimetre-scale flat-pebbles including mudstones and peloidal-rich laminated curved stromatolite fragments (Fig. 8G). The latter average between 0.5 mm and 4.0 mm in length. Some could be a superficial single layer envelope (<0.02 mm).

Environmental interpretation: Beds are laterally continuous and show normal gradations, coarser rudstone lags and subtle HCS pointing towards storm deposits. The absence of subaerial exposure features together with the occurrence of thin-bedded wavy peloidal–oolitic grainstone impacted by combined to oscillatory flows are compatible with a relatively shallow subtidal setting. The fact that this lithotype frequently contains symmetrical ripples suggests deposition within water depths between normal (fair-weather) and storm-wave base (e.g. Aigner, 1985). The intraclast composition indicates recycling of nearby lithologies within contemporaneously developed facies mosaics.

Ooid diversity: The ooids are medium to very coarse sand-size and rounded to well-rounded (Fig. 7C). The ooids are moderately to poorly sorted and the size distribution is unimodal with the grain population negatively skewed. (Table 1).

The simple multi-layered ooids with distinguishable nuclei dominate, comprising 95% of the population. The nuclei are composed of micritic intraclasts, peloids, skeletal grains (mainly ostracods), ooid fragments and a very few detrital grains (Figs. 8G, 8H and 9A). The ooids have a centred nucleus, noting eccentric types are very rare (Table 2).

The bulk of the ooids are multilayered with generally complete linings comprising light radial–concentric, fibrous–radial layers and thin dark-brown micritic layers. Broken and regenerated ooids display fragments of concentric parts of the cortex, presumably the outermost ones (Fig. 9A). In most cases, the external surface is smooth, although it may show subtle irregularities.

Compound ooids are abundant (Table 2, Fig. 9A) and consist of two, three or more individuals of different shapes and sizes (between 0.8 mm and 2.0 mm), with a matrix of micrite (dolomicrite) or fine-grained crystalline calcite. Compound ooids with more rounded shapes (*ca* 0.8 mm), show slightly thicker cortexes, with several concentric–radial fabric layers.

Cross-bedded oolitic grainstone

This lithotype occurs throughout the succession showing moderately to well-sorted cross-bedded tabular and lenticular oolitic grainstones with thicknesses varying between 30 cm and 100 cm. The bed boundaries are planar and undulated, and are frequently affected by brecciation towards the top (Fig. 5D). Individual lenticular bed-sets range between 10 to 35 cm and massive cross-bedded intervals can reach 3.5 m. Cross-

bedding usually dipping between *ca* 25 to 30° has bottom tangential terminations, alternating thickening and thinning bottomsets and finer-grained partitions, that are seldom preserved towards the toe of the distinct sets. Upper terminations are usually truncated (high-angle and sharp topsets), but metre-length sigmoidal features are also present. Massive cross-bedded sets develop more gently dipping (*ca* 15–20º) erosive reactivation surfaces yielding reverse ripples. Herringbone (bimodal) stratification is locally well-developed. Sparse bioturbation and isolated vertical tubes (*Skolithos*) are also present within this lithotype.

Lenticular cross-bedded oolitic grainstone shows poorly to moderately-sorted grains and is intimately related with *Thin-bedded mixed heterolithic bedding*. On the contrary, more tabular, better sorted and thicker cosets alternate with *Thin-bedded wavy peloidal–oolitic grainstone* and *Graded skeletal–oolitic grainstone–packstone* or *Graded intraclastic oolitic grainstone–rudstone*. The cross-bedded oolitic grainstones locally show evidence of polygonal cracking, erosion and dissolution at their tops.

Strongly yellowish to brown brecciated intervals frequently cover these oolitic grainstones forming up to 0.1 m thick caps in which a variety of clast-supported fabrics develop. Iron oxidation and dolomitization affect these intervals which are composed of angular to very angular granules, pebbles and cobbles, derived from *in situ* exhumation of the grainstones below.

Isolated or laterally-linked (patch-like) domal stromatolites with clear hemispheroidal (synoptic) relief with as much as 0.30 m amplitude and varying between 0.2 to 1.0 m in length developed coevally and are intimately associated with the above-described facies. In planform the stromatolite domes frequently show subparallel oriented elongated shapes. Internally, they develop various fabrics differing between finely laminated and thrombolitic textures.

Composition: This facies contains >85% bimodal mixtures of fine and coarse-grained ooids including compound types, <5% bioclasts, (ostracods, and frequently reworked bivalves and gastropods) and 5 to 10% intraclasts. The grains can either be isolated or grouped and floating within the grainy matrix or forming rudstone lags. The intraclasts include grainstones, packstones and stromatolite fragments with irregular shapes but rounded edges. Rounded and very rounded sand-sized monocrystalline quartz grains are also present comprising up to 5%.

Environmental interpretation: The two different types of cross-bedded oolitic grainstones described are interpreted to represent active bed loads deposited in relatively high energy marine environments, wherein thicker cosets or recurrent relatively tabular bodies represent subtidal shoals (dune complexes) with clear tidal influence, whereas the more lenticular bodies represent tidal-flat channel fills (e.g. Demicco & Hardie, 1994; Lasemi *et al.,* 2012; Pérez López & Pérez Valera, 2012). Cross-beds represent active two-dimensional to three-dimensional dunes associated with tidal and littoral currents within a shallow marine setting. Intimate lateral relationships with microbial domes and patch-reefs are found. The frequent weathering (colour change and oxidation) and brittle brecciation at the top of these grainstones suggests periodic subaerial exposure. Local reworking and fine particle winnowing are common and generate a variety of coarse-grained lags.

Ooid diversity: Within this lithotype ooids have a wide size range and morphological diversity (Fig. 9B to O). A large variety in both simple multilayered and compound types co-occur (Table 1).

Ninety percent of the simple multilayered ooids have identifiable subrounded to rounded centred nuclei with sharp to slightly irregular edges; the rest display undeterminable nuclei (Table 2, Fig. 9B to D). Small nuclei mostly consist of peloids and quartz grains because bigger nuclei include bioclasts, largely gastropods, bivalves and ostracods, some of the nuclei are partly affected by early diagenetic features. This lithotype shows moderate to poorly-sorted ooids, with a negatively skewed bimodal distribution and roundness indicating subrounded to well-rounded ooids (Fig. 7D, Table 2).

Superficial ooids are poorly represented and copy the shape of the nucleus (Table 2). The cortex of simple multilayered ooids consists of radially arranged calcite crystals in concentric envelopes with as much as 25 linings. Festoon–cerebroid ooids dominate and can exceed 70% (Fig. 9D, 9E, 9I, 9K and 9L). In addition, smooth and rare crenulate surfaces are present. Festoon shapes show relatively thick even cortexes (0.02–0.25 mm), with internal fan-shaped crystal bundles or sets of fibro-radiated or bladed crystals with frequent fascicular optic extinction (Kendall, 1977), alternating with micritic dark bands. Fan-shaped crystals reach the external surface where they protrude distinctly as convex bulges or are flat-topped, some of which resemble micro-domal to columnar

features (Table 2, Fig. 9I). Festoon ooids may vary from strongly crenulate to smooth outer outlines and vice versa. This crenulation occurs gradually after several laminae or abruptly without transition and is marked by truncations or sudden compensation of microreliefs (Fig. 9D and I). A slightly darker irregular micrite rim is identifiable accompanying this feature. (Fig. 9I). Thickness variations of the envelopes resulted in better rounded ooid shapes, whereas others developed more irregular or amebiform geometries (Table 2).

Within simple ooids half-split or split-off portions of the envelopes, presumably the most external ones, represent broken and regenerated ooids (Table 2, Fig. 9F and H, *ca* 5 %). Two types of regeneration were present. The first type showed fragments that after breaking were worn-out (i.e. eroded) and then enveloped again by multiple-layers with the same fibrous–radial fabrics as shown by the other ooids. The second type displayed some fragments that did not regenerate and these remained as loose pieces with a freshly broken appearance (Fig. 9I). Also, within simple ooids, angular internal unconformities, including tangential truncations or partial subtraction of various lamina, show further onlap and lap-out relationships. In festoon forms this feature was also observed; perhaps more evident given the strong change in curvature radius (Fig. 9I).

Different samples of this lithotype show compound ooids with amounts varying between 6% and 90% of the sample. Some of the compound ooids have complex nuclei with sizes ranging from 1 mm to up to 4 mm (Table 2). Larger compound layered grains yield very irregular morphologies that contrast with the most common spherical shapes of simple ooids (Fig. 9G and K to O). Compound ooid types include a variety of nuclei that consist by clusters of two to four individual ooids, micritic intraclasts peloids and/or detrital grains. Large compound grains show a calcite meniscus on their concave side similar to septa which connect both sides (Fig. 9K). They may also develop festoon–cerebroid forms and sometimes show directional growth (Fig. 9N) and internal zebra-like mottling (Fig 9K to L). Clusters of simple and compound ooids, together with micritic intraclasts and detrital quartz grains, can form the nuclei of more complex grains (Fig. 9G) or even be included within the cortex (Fig. 9O). Some of them even show cumulative accretion and lining with two, three, four or more grains, being ooids themselves. These grains show a different degree of roundness ranging from types with evident local internal discontinuities (that compensate relief) to very irregular and enveloped by even layers.

Thin-bedded mixed heterolithic bedding

These sediments represent a thin to very thin-bedded heterolithic facies (sandy ribbon limestones) with variable sand/mud ratios and flaser to wavy bedding, characterized by pinch and swell along bedding planes (Fig. 5E and F). Sediments comprise sandy peloidal–oolitic limestones whereas muds are partly carbonate (mudstones to wackstones) and partly yellowish marls. Alternating thin flaser dominated intervals and more lenticular intervals occur, and minor laterally discontinuous flat-pebble conglomerate partitions are also present. Moreover, bundles of alternating very thin and thicker laminae are also present, some of which seem micro-crenulate and resemble biolaminites. Greenish recessive shale partitions with silty–sandy laminae also occur, including very well-rounded quartz grains with thin reddish oxidized layers. The complete interval of this lithotype displays internal ripple-lamination with alternating (bimodal) flow directions. In plan view, interference ripple patterns are common as well as double crests and flat-topped (truncated) symmetrical ripples. Superimposed on the entire association, 'V' shaped features (Fig. 5F) with depths up to 10 cm and sandy fills are present and their plan view reveals two main types: (i) well-developed partly superposed complete polygons of various sizes; and (ii) incomplete pseudo-polygonal cracks with detached triple points or short double ended cracks with less contrasting infill. Complete polygons vary in shape and in size, from a few centimetres to decimetres. They clearly develop in mud drapes in between sandier beds and are filled with contrasting grain sizes. *Thalassinoides* burrows locally develop 3D frameworks in this lithotype that laterally pass into more intensively bioturbated beds. The diversity of ooids in this facies is similar to that of the *Thin-bedded wavy peloidal–oolitic grainstone* facies (Fig. 8A to C, Table 2).

Environmental interpretation: Typical recurrent thin-bedded flaser to wavy heterolithic bedding has been suggested to characterize tidal flats with alternating traction and settling processes (Demicco & Hardie, 1994; Bayet-Goll *et al.,* 2015; Lehrmann *et al.,* 2020). Flattened ripple crests, interference patterns developed along ripple valleys and clear features of desiccation (pervasive and recurrent mud cracking), indicate episodic subaerial exposure and a marginal setting for this facies association, which is also consistent with burrow patterns. Pervasive bimodal flow directions are consistent with tidal influence (Lasemi *et al.,* 2012).

ENVIRONMENTAL PROCESSES CONTROLLING OOID DIVERSITY IN THE YACORAITE FORMATION

Numerous processes are involved in ooid formation and those that have been recognized in the Yacoraite Formation ooids are summarized in Table 3. The processes involved are controlled by the depositional environment (for recent reviews see Trower *et al.,* 2017, 2018, 2020, Mariotti *et al.,* 2018; Diaz & Eberli, 2019; Harris *et al.,* 2019; Anderson *et al.,* 2020) and, although they may characterize different environmental settings, the environmental dynamics dictate the way in which these processes change in space and time. Thus, dominant processes will be implicitly shown by the microfabric of the ooids: (i) persistent high-energy conditions (cf. Trower *et al.,* 2017); (ii) episodic or periodic hydrodynamic changes (cf. Mariotti *et al.,* 2018; Anderson *et al.,* 2020); and (iii) subaerial exposure (Eardley, 1938, Purser & Loreau, 1973; this study). These processes may produce a variety of ooid microfabrics, shape and size distributions in the resulting oolitic deposits.

Constructive and destructive processes involved in laminae accretion and ooid formation occur during the ***suspension/transport mode*** (Trower *et al*., 2017) or throughout the ***benthic/marine phreatic mode*** (Mariotti *et al*., 2018, Anderson *et al*., 2020) (Fig. 10, Table 3). Whereas constructive processes result in carbonate precipitation and ooid lamina accretion (thus ooid growth), destructive processes result in physical or chemical modification and/or degradation of the laminae, including abrasion, microboring and corrosion (Table 3). Although vadose–subaerial processes are not usually considered during ooid formation, these can also influence ooid binding, wearing and breakage (characteristics and textures included within the ***vadose–subaerial mode***, Table 3). The latter mode may similarly apply in settings with limited accommodation and high-frequency, strong periodic or episodic environmental changes, such as subaerial exposure related to tidal dynamics and/or sudden storm related changes.

The alternation between the suspension/transport mode, benthic/marine phreatic mode and vadose/subaerial mode during recycling is important because it increases the morphological and textural complexity of ooids, as shown by quantitative data. Such complexity linked to alternating modes is evident in the textural diversity and complexity

of the Yacoraite Formation ooids. The variability, although implicitly shown by ooid microtextures and fabrics, together with shape and size distributions, can help to improve the interpretation of the depositional environment. Thus, paraphrasing Dott (1983), the question is whether the sedimentary record of oolites in the Yacoraite Formation reflects ordinary day-to-day processes that acted uniformly through time, or whether they record rare or even extraordinary processes that acted intermittently? The approach discussed in this study may be particularly useful when working with limited information such as drill cores or cuttings when microtextural aspects become important and are the main source of information. The textural diversity of the ooids in the Yacoraite Formation and the processes involved are summarized in Fig. 10 and Table 3, and are described in the next section.

Suspension/Transport mode

When chemical conditions are favourable (carbonate saturation state Ω>>1), nuclei are available and persistent water agitation dominates (relatively high-energy conditions sustained over time) ooids may naturally occur (Fig. 10, stages a to b). In the Yacoraite Formation, these environmental conditions apply to the thin-bedded wavy peloidal–oolitic grainstone lithofacies (Fig. 7A). As expected, within this lithofacies, ooids are relatively well-sorted, and simple ooids predominate showing a symmetrical unimodal size distribution (Fig. 7A). The ooid features, as indicated by quantitative analysis, agree with their formation under high-energy hydrodynamic conditions with persistent agitation where ooid growth results from the net balance between lamina accretion and abrasion. Under these conditions, ooids may reach an *equilibrium size* as suggested by Trower *et al*. (2017). Thus, if particles stay long enough within a relatively high-energy oolite belt, they will develop shape and size distributions as extensively discussed in recent papers by Trower *et al.* (2017, 2018, 2020). This pattern was also found in the thin-bedded wavy peloidal–oolitic grainstone of the Yacoraite Formation (Fig. 7A to C). Under these sustained agitation conditions, ooids will become progressively enveloped with multilayers (Fig. 10, stage c) and can develop thinning or thickening outward lamina trends (Fig. 1). The Yacoraite Formation thickness trends show both thinning, thickening outward and random lamina trends, but the underlying processes cause these variations to remain unclear. Sipos *et al*. (2018), suggested that thinning outward trends may

indicate increasing abrasion relative to precipitation as ooids grow. Such a pattern may also develop due to the need of maintaining equal volume (equal area) distribution at constant precipitation rates. Alternatively, Batchelor *et al*. (2018), hypothesized that a biological influence on ooid growth could be responsible for decreasing laminae thickness, at uniform time intervals under constant microbial parameter growth conditions together with constant mineralization rate.

Smaller ooid sizes and smooth external surfaces were observed in some samples (Fig. 8A to C), which may indicate that suspended load transport predominated (Heller *et al.,* 1980; Trower *et al.,* 2018); this is consistent with the abundance of spherical shapes (Sipos *et al.,* 2018). In contrast, elongated shapes observed in the graded–skeletal–oolitic grainstones and packstones lithotypes are not necessarily associated with rolling transportation in a coarse-grained bed-load (Domokos *et al.,* 2014; Sipos *et al.,* 2018), but may have a strong shape inheritance associated with the presence of bioclastic nuclei (Fig. 8D and E). The diversity of sizes and shapes of the bioclasts involved within these lithotypes, including abundant small ostracods and larger fragments of bivalves and gastropods, leads to smaller rounded ooids and larger elongated ooids, respectively. These differences in available nuclei also translate into a slightly different size frequency distribution in this lithotype (Fig. 7B).

Benthic/marine phreatic mode

If ooids drop-off or become excluded from the high-energy belt, and are placed under low-energy conditions (benthic/marine phreatic stage, *case 1*, Table 3), other processes may induce lamina accretion, for example where microbial biofilms can trigger carbonate precipitation and thus ooid growth (cf. Diaz *et al*., 2017, Plee *et al*., 2008; Pacton *et al*., 2012; O'Reilly *et al*., 2017; Mariotti *et al*., 2018). The aforementioned process may produce textural modifications, but also result in particle aggregation associated with bacterial colonization and biofilm development, as suggested by Mariotti *et al*. (2018) in their benthic accretionary model. This process may explain the various features observed and described for the Yacoraite Formation ooids, like the laminae textural changes and micrite-rich laminae. Other features might also relate to this process, such as: (i) the surface modified grains (for example, those affected by corrosion, pit development, micritization); (ii) irregular growths and inclusions (Fig. 9I, N

and O); as well as (iii) amalgamation (grapestone) and bonding between ooids or ooids and other grains (precursors to compound ooids). These processes must occur before high-energy conditions return (Fig. 10, stage c) and renewed lining results in a more diverse size and shape distribution, now including some ooids with multiple nuclei. According to Mariotti *et al*. (2018) the benthic growth mechanism can predominate when granular material is shed to slightly deeper (for example, below fair-weather wave base) or calm waters (for example, lagoonal) for prolonged periods of time. The abundance of microbialites (stromatolites) in the Yacoraite Formation, closely associated with the ooid-bearing lithotypes, supports the idea that biofilm development and microbially-mediated laminae accretion (and thus benthic growth) could have been an important process for ooid growth processes recorded in the Yacoraite Formation. Lamina accretion during benthic/marine phreatic growth, in a low-energy calcium carbonate oversaturated setting, without the influence of significant microbial activity, could also contribute to the *in situ* growth of ooids but such ooids will significantly differ (showing a different microtexture) from the biofilm-mediated growth patterns (Paradis, 2019). The lobate, festoon–cerebroid shapes developed in the cross-bedded oolitic grainstone lithotype (Figs 9B to F, 9I, 9K, 9L and 10, stage d) may have resulted from *in situ* growth processes, because they lack significant abrasion, which is consistent with lamina accretion in a quiet, low-energy setting. Simple and compound multilayered ooids formed within this stage strongly differ from the smooth and rounded shapes that characterize the agitated environment (stage c), where both collision and traction induced abrasion controls laminae development thickness changes, shape compensation and internal discontinuities (Fig. 9J) (e.g. Sipos *et al*., 2018). As observed in Fig. 9, lobate, festoon–cerebroid textures occasionally alternate with micrite-rich irregular laminae. This alternation suggests that, during benthic growth, both mechanisms (biofilm-mediated versus more abiotic precipitation) may have contributed to lamina accretion in the Yacoraite Formation ooids.

Additionally, ooids could also grow and accrete laminae when resting in the marine phreatic environment (within the sediment pile, below the sediment–water interface), not necessarily exiting a high-energy belt but affected by episodic/cyclical recycling (repeated ooid burial, exhumation and transport), as suggested by Anderson *et al*. (2020) (see *case 2* in Table 3); in this bedform model, if residence time is long enough, the precipitation of marine cements within the sediments (serrate or irregular fringes around grains and

towards pore spaces) under high porewater carbonate saturation can occur and thus contribute to ooid growth. According to Anderson *et al*. (2020), this can occur particularly during times of low O_2, low organic matter and/or high carbonate saturation in surface seawater. These cements will be exposed to abrasion, rounding and smoothing when exhumed and exposed in the high-energy zone, the net result being lamina accretion (Table 3, see Anderson *et al.*, 2020). The authors cannot discard ooid growth through a similar mechanism (within the sediment as proposed by Anderson *et al*., 2020) if local carbonate oversaturation occurs within the sediment pile (not necessarily meaning widespread surface seawater saturation and/or anoxia, as proposed in the original model). In the Yacoraite Formation this mechanism could potentially explain some radial fibrous textures (Fig. 9H).

When aggregates formed during the benthic/marine phreatic mode are subjected to renewed sustained higher-energy conditions (wave or tidally induced) (Fig. 10, stage c), new lamina accretion may start increasing the ooid size. Distinct compound ooids develop during this stage. Moreover, alternations of irregular micrite and crystalline laminae, as well as corroded, crenulate external features, instead of successive simple smooth surfaces, indicate recurrent repose or benthic modes, allowing the development of micrite laminae associated with either microboring impact or microbial colonization.

After early or incipient cementation (Fig. 10, stage e), which can take place entirely subaqueously (partly phreatic, stage e) or partly subaerially (including vadose, stage h), further reworking and growth can occur on both single and compound ooids. In complex littoral environmental mosaics, sediment reworking may occur through various mechanisms: (i) subaerial exhumation–erosion or subaqueous-erosion associated with storms; (ii) unusual tidal ranges; or (iii) minor high-frequency sea-level fluctuations. If surface cementation is incomplete or weathering takes place disaggregating the substrate, new compound grains can be formed (Fig. 10, stage f). These ‘intraclasts’, in turn, can be incorporated into the ooid conveyor belt again and then may become the nucleii of new compound ooids as observed in some cases (Figs 9F and 10, stage g).

The presence of abundant large simple festoon–cerebroid ooids (Fig. 9B to F, I, K and L) and diverse simple and compound ooids in cross-bedded oolitic grainstone and in the graded intraclastic–oolitic grainstone–rudstone is interpreted as a result of textural mixtures associated with storm processes, reworking and recycling (Figs 8F to H and

9A). Back and forth loops between different stages (d and c or b) can occur repeatedly in order to mix components prior to final cementation (Fig. 10, stage e).

Vadose/subaerial mode

Other features observed in the Yacoraite ooids that relate to lamina accretion could have a vadose or subaerial origin. A wide variety of compound ooids accompany multilayered simple ooids particularly within the graded intraclastic–oolitic grainstone–rudstone and the cross-bedded oolitic grainstone, which also show a great number of intraclasts (up to 35% – mostly fragments of oolite grainstones). Compound ooids show a great variety of sizes, external shapes, internal features, and various individual bonded components (at least one being an ooid) and repeated linings (Figs 8 and 9). Cements with eccentric, pendant and lateral growth as well as localized meniscus cement occur associated with the compound ooids. These features originate from vadose and subaerial processes generating composite–aggregate grains. Eardley (1938) termed such features, occurring in deposits from the Great Salt Lake (Utah), hydrogenic shingles, and Purser & Loreau (1973) named them boulder-gravelly pisoliths, which they described from the sabkhas of the Trucial Coast on the Persian Gulf. Some of the Yacoraite compound grains resemble the irregular pisoids described from intertidal to supratidal subenvironments (associated with beach-rock) within the Persian Gulf (Loreau & Purser, 1973; Purser & Loreau, 1973) whereas others contain asymmetrical features resembling vadoid (Dunham, 1969; Esteban & Pray, 1983) and arborescent encrustations (Risacher & Eugster, 1979). Compound grains can thus develop either when granular material is shed towards slightly deeper water (enhancing aggregation and grapestone formation) or when grains are exported out of the high-energy belt (for example, the surf–splash zone) to supratidal areas (or alternatively, eulittoral–supralittoral when lacustrine, *cf*. Arp, 1995) and become incorporated within subaerial–vadose environments. Eardley (1938) discussed that theses compound grains in subaerial environments are cemented chiefly by precipitation from solution, but the Yacoraite ooids suggest that pendant and lateral cement precipitation observed in the samples may result from wind spray and successive capillary processes (Fig 9G and K). These two very common processes increase particle binding and may add to new lamina accretion (e.g. Gomez *et al.,* 2014), thus leading to compound ooid formation along coastal plains, when particles are subaerially exposed

(Fig. 9G). Within low-gradient coastal environments in epicontinental seas (for example, salt coastal) or on lacustrine plains (eulittoral–supralittoral), ooids can remain dormant for long periods, and may become partially cemented, which results in the formation of very irregular geometric surfaces and shapes. Particularly irregular overgrowths and eccentric development, localized dissolution embayments and meniscus formation seem diagnostic of subaerial–vadose processes (Figs 9K to O and 10, stage i); features that can be discerned by detailed petrographic observations (e.g. Scholle & Ulmer-Scholle 2003; Belkhedim *et al*., 2019). Vadose features (Fig. 10, stages h, i and j) have also been linked to pedogenetic processes, where dissolution, recrystallization and 'grainification' (Freytet, 1973; Arp, 1995; Freytet & Verrecchia, 2002; Glumac *et al.,* 2012) characterize and may further influence composite grains (e.g. Peryt & Piatkowski, 1977; Mazzullo & Birdwell, 1989). All particles formed in the vadose/subaerial environment can be remobilized in the high-energy zone and can be layered (Fig. 10, stage k), thus forming more complex ooids (Fig. 10, stage m). Renewed lamina accretion may alternatively occur after some erosion and rounding (Fig. 10, stages g and k). Conversely, if composite particles happen to add lamina in a relatively quiescent environment, they may replicate their inherited shape and prevent rounding (Fig. 10, stage j).

The presence of broken ooids and regenerated ooids (Fig. 9F and H), suggests brittle ooid breakage and partial rounding before layering (Fig. 10, stage l). Broken and re-layered ooids are rare in high-energy open-marine subtidal environments (Husinec & Read, 2006) but abundant in lacustrine settings and carbonate aeolianites (Sandberg, 1975; Hunter, 1993; Caputo, 1995; Flügel, 2004, McGuire, 2014). The broken ooids may result from expansion and contraction due to heating and cooling, respectively, or find their origin in strong grain-to-grain collisions during aeolian transport. Alternatively, vadose dissolution can also generate similar apparent features like half-size ooids (Smith, 2019), requiring exhumation–erosion and later incorporation back into the subaqueous saturated environment to allow further ooid growth.

DISCUSSION

Environmental variability in Yacoraite Formation ooids

Detailed analysis of the diversity of ooids from varying environmental conditions and settings within the Yacoraite Formation sediments advances discussion regarding the

marine versus lacustrine origin of these deposits (Marquillas *et al.,* 2005, 2007; Tasistro-Hart *et al.,* 2020; Deschamps *et al.,* 2020; Gomes *et al.,* 2020). The documented size distribution, shapes and astonishing diversity of microtextures documented within the Yacoraite Formation oolites, makes them difficult to reconcile with a simple equilibrium ooid size distribution model, as observed in classic high-energy marine environments (as discussed by Trower *et al.,* 2017). Our facies analysis suggests a different environmental setting for the Bahamian-type ooid shoals with subtidal high-energy environments largely sustained over time (Illing, 1954; Bathurst, 1975; Davies *et al.,* 1978; Simone, 1981; Strasser, 1986; Tucker & Wright, 1990, Flügel, 2004; Rankey & Reeder, 2011; Trower *et al*., 2018; Harris *et al*., 2019). Although our facies assemblage indicates shallowing upward cycles with both wave and tidal influence with recurrent exposure, only the well-rounded, simpler and better-sorted ooids observed in the Yacoraite Formation (particularly, *Thin-bedded wavy peloidal–oolitic grainstone* and *Thin-bedded mixed heterolithic bedding* lithotypes) have reached an equilibrium size under a sustained agitated subtidal environment (*cf.* Trower *et al.,* 2017). On the contrary, most of the Yacoraite Formation ooids are characterized by unusually diverse, complex and composite morphologies. Our literature review provides an opportunity to establish comparisons with other ancient examples (Beukes, 1983; Husinec & Read 2006; Lehrmann *et al.,* 2012; Mei and Gao, 2012; Li *et al.,* 2019) that also seem to yield a wide variety of morphologies (for example, broken and regenerated ooids in aeolian environments, cerebroid ooid giant morphologies in vadose environments, and unusually highly saturated marine environments).

Within the Yacoraite Formation, superficial as well as simple multilayer ooids develop over a diversity of detrital siliciclastic components, bioclasts or peloids (as a nucleus), compatible with the equilibrium size theory of Trower *et al.,* 2017, 2020. However, a different set of more complex and diverse processes (Table 3) seem to control lamina accretion on composite grains. The development of envelopes with uneven thickness, festoon and ameboid ooid types, and irregular, micrite-rich lamina development (possibly related to microbial activity within biofilms), clearly suggest stages of net ooid growth with limited abrasion. Additionally, during the benthic stage, early diagenetic processes enhanced local cementation, binding and merging between single ooids (and other components, Fig. 9M to O). The variety of compound ooids, and

recorded sizes and shapes is difficult to reconcile with commonly suggested abrasion dynamics (*cf*. Trower *et al.,* 2017).

The variety of benthic processes present (Fig. 10) would also occur in a lacustrine environment where hydrodynamic conditions are more variable and may strongly differ from high-energy marine shoal belts. The concept of a high-energy shallow-water *conveyor belt* developed by Mariotti *et al.* (2018) suggests that ooids become segregated out of the surf zone (beach and shoreface environment as in Cat Island, Bahamas), exiting the high-energy regions where abrasion and rounding strongly dominate. This process allows ooids to grow in response to different mechanisms operating in lower energy settings, influenced by microbial activity (Freeman, 1962; Mariotti *et al.,* 2018; Mariotti & Fagherazzi, 2012). The aforementioned sedimentation process matches with the frequent aggregation into larger particles, which together with other textural characteristics, such as ooid laminae with no clear trend in the change of thickness, ooid laminae with external irregularities and ooids that include multiple nuclei, suggest processes of ooid aggradation. (Mariotti *et al.,* 2018). However, the various ooids from the Yacoraite Formation still depart from those described by Mariotti *et al.* (2018). Irregular ooids including simple festoon–cerebroid, aggregates and compound types are very common in the Yacoraite samples (*Graded skeletal–oolitic grainstone–packstone, Graded intraclastic oolitic grainstone–rudstone* and *Cross-bedded oolitic–grainstone* lithotypes). The simple (superficial and multilayer) ooids present frequently retain a nucleus shape which implies that little significant rounding occurred. Replicating the original nucleus shape agrees with limited abrasion and agitation processes (cf. Trower *et al.,* 2020), such as avoiding high rounding rates. Experimental data and direct observations by Mariotti *et al.* (2018) suggested that small surface irregularities on simple or compound ooids can be abraded within days, once ooids resume movement. Although the present study observed rounding patterns and unconformity development in some of the ooids, it does not seem to be the norm, but rather the exception. Alternative paths or loops implying higher intricacy and recurrent mixtures as well as unusual vadose–subaerial processes may possibly explain the diversity and complexity of the ooid populations in the Yacoraite Formation.

The presence of grapestones (Purdy, 1963), and varieties of aggregate grains originally described as ‘lumps’ by Illing (1954), requires a set of different environmental

conditions allowing binding and/or cementation of ooids and other particles. These processes imply water energy fluctuations and periods with protected bottom stability (Winland & Matthews, 1974). Grapestone usually breaks down by abrasion in highly energetic settings unless enough repose time allows the development of mature crusts (Illing, 1954; Van Ee *et al.,* 2008). Although grapestones are a variety of aggregate grains (Purdy, 1963), they were originally described in the seminal paper by Illing (1954) on the Bahamas in which various kinds of 'lumps' with different degrees of cementation were discussed. In an attempt to better characterize grapestones, Taft *et al.* (1968) separated several varieties (that apparently constitute a continuum) based on the surface area of the particle covered by cement. Those authors also added that, within incipient grapestones, cement was largely restricted to the surface of the aggregate, whereas the interior remained fairly porous. If cement (as an isopachous rim) discontinuously covered less than 50% of the aggregate, the grains were classified following Illing (1954) as firmer aggregates. When rounding and cementation increased, both in the interior and over 50% of the particle was layered with cement, the grain was classified as well-cemented grapestone. Moreover, Taft *et al.* (1968) noted that with continued accretion, cement completely covered the aggregate grains, resulting in a smooth, better rounded, layered-grapestone in which the constituent particles are detectable beneath the cement and protrude through the surface reducing sphericity. Similarly, when the ooids repeatedly abrade and accrete outward, their irregular appearance gradually disappeared and they turned into well-rounded composite grains. The latter pattern is shown in samples of subtidal lithotypes *Graded intraclastic oolitic grainstone–rudstone* and *Cross-bedded oolitic grainstone* including mixtures of various degrees of 'maturity'. Moreover, grains with a third and fourth generation were counted, implying multiple re-layering phases after incipient grapestone development. Taft *et al*. (1968) discussed that such a variety of grains predominate the bulk of the carbonate grains occurring at water depths of less than 3 m on the New Providence Platform (Bahamas) situated between Tongue of the Ocean and Exuma Sound.

Newell *et al*. (1960) described an evolution from single superficial ooids into more mature, multilayered ooids for Brown's Cay (Western Great Bahama Bank, Bahamas). In the Yacoraite Formation this progression is preferentially shown in the lowermost section (see Fig. 3), but a similar tendency is displayed by intraclasts within the upper intervals of

the oolitic rudstones and grainstone/rudstones lithotypes. Intraclasts within rudstones show progressively thicker isopachous lamina development, to a point where discriminating between relatively small (<5–10 mm) intraclasts and large composite ooids becomes extremely difficult, because they clearly overlap in size and both show incipient to pervasive lining and similar roundness.

Many of the recorded textures in the Yacoraite Formation are strikingly similar to those described for ooids from the Great Salt Lake (Eardley, 1938, Carrozzi, 1962; Halley *et al*., 1977; Chidsay *et al*. 2015; Paradis *et al.,* 2017; Paradis, 2019; Trower *et al.,* 2020; Ingalls *et al.*, 2020; Smith *et al.*, 2020). In addition, some features are comparable to the incipient growth stages observed in Lake Geneva ooids (Davaud & Girardclos, 2001; Plee *et al.,* 2008; Ariztegui *et al.,* 2012). Great Salt Lake and Lake Geneva present contrasting environmental conditions (water depth and hydrochemistry). Similar ooid patterns may suggest analogous processes during ooid growth, but not necessarily a lacustrine environment, because ooids and processes described for marine environments by Mariotti *et al.* (2018) and Purser & Loreau (1973) also resemble many aspects of the ooids documented in the Yacoraite Formation, for example size and morphology.

The ooid diversity in the Yacoraite Formation stresses the fact that environmental variability and recycling are standard features, which are probably related to limited accommodation (see next section). Higher intermittency and frequent exposure may result in the observed ooid diversity. Although lacustrine ooids are shaped by different processes, and apparently include a higher diversity assemblage of ooid morphotypes than marine ooids, such variability could also be produced in tidally influenced environments or highly dynamic lacustrine and coastal saline ponds.

Ooid growth and recycling in settings with limited accommodation

The study suggests that the vast majority of ooid types present in the Yacoraite Formation have largely non-equilibrium shapes. These ooids were probably formed under highly unstable and variable environmental conditions and evolved following diverse paths and processes, as shown in Fig. 10. The different trajectories proposed can be interpreted to occur within a given sample, suggesting time-averaging processes (Kidwell, 1998), particularly when a diversity of compound ooid types appear together. Complex environmental mosaics (as opposed to stable subtidal high-energy conditions

like in the Bahamas, Rankey *et al.,* 2006; Rankey & Reeder 2011; Trower *et al.,* 2018; Harris *et al.,* 2019), enable mixtures to develop and reduce the overall sorting and homogeneity among ooid types.

The population analysis of the Yacoraite Formation ooids showed: (i) variable sorting (bimodal and polymodal distributions); (ii) a diversity of shapes; (iii) varying lamina textures; and (iv) different particles acting as the nucleus. This assembly of population characteristics indicates recurrent mixing and intermingling of ooids that followed different evolving paths and lamina accretion/destruction processes (Fig. 10). The significant number of compounds ooids (5–35%), some showing various dissolution features, meniscus development and repeated envelope generations, together with layered oolite intraclasts, strongly suggest that exposure, cementation and recycling related to limited accommodation characterized the depositional environment. Reworking of the simple ooids is indicated by eccentricity, growth compensation, subtle internal unconformities and broken/regenerated ooids. The presence of clean sharp surfaces and low-angle truncations in some of the multi-layered simple and festoon–cerebroid ooids is interpreted as erosional discontinuities due to reworking. The fact that broken regenerated ooids commonly occur within the deposits (for example, graded intraclastic oolitic–grainstone–rudstone and cross-bedded oolitic grainstone) confirms that these deposits were frequently subjected to subaerial exposure processes. Similar characteristics were described from transgressive carbonates (Husinec & Read, 2006), in which ooids that were originally formed in coastal hypersaline ponds in arid environments were affected by wind and vadose processes. At a later stage, these sediments were subject to rising sea level, that favoured ooid recycling. Similar features have also been recorded in arid dynamic lacustrine systems such as the Great Salt Lake (e.g. Chidsay *et al*. 2015, Ingalls *et al*., 2020). Strasser (1986) and Glumac *et al.* (2012) discussed ooid complexity and recurrent layering, and attributed repeated accretionary stages and recycling to little available accommodation. Strasser (1986) argued that superposition of various cortical patterns (his type 6 ooids) reflected gradual or abrupt changes in hydrodynamic regimes, water chemistry and/or microbiological activity. Such changes were caused by shifting coastal morphologies and strong climatic forcing, influencing water chemistry through evaporation or rainfall in phreatic and vadose environments. Strasser (1986) stressed that high-energy events (storms) were capable of mixing water and sediment from

various sources. All of these alternative variations demonstrate that little accommodation is needed to facilitate the development of a range of processes within the same stratigraphic interval. These environmental requirements are met in the Yacoraite depositional setting as confirmed by the ooid variability encountered in these deposits.

Recognition and awareness of complex ooid characteristics and ooid variability may be the only information available when studies are made based on the limited amount of data retrieved from well cores or cuttings. The new classification scheme may provide alternative realistic interpretations. Low accommodation may favour frequent reprocessing and recurrent recycling (Fig. 10) within complex environmental mosaics, which will be maximized within low-gradient epicontinental settings (e.g. Pérez López & Pérez Valera, 2012). The present Cretaceous case study shows superposition of various physical (chemical) and biotic processes, which may be the norm in the fossil record. Mixing and preservation of different ooid types may be the key to interpreting palaeoenvironmental variations over short timescales, whereas recycling and superposition of recurrent constructive and destructive ooid processes might indicate longer-term time-averaged sedimentological condensation (Gómez Férnandez & Fernández López, 1994; Kidwell, 1998; Lehrmann *et al.,* 2020), which can be of importance for sequence stratigraphic interpretations.

SUMMARY AND CONCLUSIONS

Qualitative ooid types and quantitative ooid patterns (sizes and shapes), as well as textural mixtures present in the Cretaceous ooids of the Yacoraite Formation (Argentina), reflect various processes related to frequent switching energy levels and recurrent constructive–destructive stages. Quantitative data supports the interpretation of simple ooids forming under equilibrium conditions and the more complex ooids forming under non-equilibrium conditions. Additional lamina complexities present within simple multilayered ooids and the diversity of compound types suggest recycling, time-averaging processes in a depositional environment with little accommodation.

Simple multilayered ooids including the cerebroid–festoon ooids from the study area show great similarities with morphologies of ooids that currently are present within the Great Salt Lake in Utah (Kahle, 1974; Trower *et al*., 2020, and references therein). However, a whole set of compound forms distinct from the Cretaceous ooids deviate from

this pattern showing a high number (35%) of intraclasts and recycled oolites (this includes fragments of oolitic grainstones and of individual broken ooids). The ooids even display second, third and fourth-order recycling patterns reflecting recurrent ooid generation, and possible vadose processes indicating periodic emergence. This recycling pattern marked by internal discontinuities, recrystallization and thin lining growth implies much stronger disruptions between constructive and destructive stages as observed in marine Bahamian ooid archetypes.

In conclusion, the variety of ooids found in the Cretaceous Yacoraite Formation display significant similarities with an ooid spectrum produced in a lacustrine setting that at times was influenced by marine processes, as shown by various sedimentological features, for example, bi-directional cross-bedding, tidal shoals and hummocky cross-stratification (HCS). Hence, the depositional realm resembles a shallow coastal lagoon with distinct lacustrine characteristics that at times was subjected to prolonged marine incursions.

ACKNOWLEDGEMENTS

Funding and support were provided by the CICTERRA (Centro de Investigaciones en Ciencias de la Tierra), the CONICET (Consejo Nacional de Investigaciones Científicas y Técnicas), project PIP11220150100664CO to F.J.G., and the SECYT (Secretaría de Ciencia y Tecnología–Universidad Nacional de Córdoba), projects 30720130100119CB and 33620180100911CB to R.A.A. We thank Emiliano Rivarola for field assistance. We acknowledge the technicians of the CICTERRA for their continuous work to promote and develop high-level scientific research. We specially thank reviewers Gene. Rankey (Kansas), Daniel Lehrmann (San Antonio), an anonymous reviewer, and Associate Editor Prof. John Reijmer (Amstelveen) for their very valuable revisions that greatly improved the final version of our paper.

DATA AVAILABILITY STATEMENT

The data that support the findings of this study are available from the corresponding author upon reasonable request.

REFERENCES

Aigner, D.K. (1985) Storm depositional systems: Dynamic stratigraphy in modern and ancient shallow-marine sequences. *Lecture notes in Earth Science*, **3**, 174pp.

Anderson, N.T., **Cowan, C.A.** and **Bergmann, K.D.** (2020) A case for the growth of ancient ooids within the sediment pile. *J. Sed. Res.,* **90**, 843-854.

Ariztegui, D., **Plee, K.**, **Farah, R.**, **Menzinger, N.** and **Pacton, M.** (2012) Bridging the gap between biological and sedimentological processes in ooid formation: Crystalizing FA FOREL's vision. *Archives des Sciences*, **65**, 93-102.

Arp, G. (1995) Lacustrine bioherms, spring mounds, and marginal carbonates of the Ries-impact-crater (Miocene, southern Germany). *Facies,* **33**, 35-89.

Barrett, P.J. (1980) The shape of rock particles, a critical review. *Sedimentology*, **27**, 291-303.

Batchelor, M.T., **Burne, R.V.**, **Henry, B.I.**, **Li, F.** and **Paul, J.** (2018) A biofilm and organomineralisation model for the growth and limiting size of ooids. *Scientific reports*, **8**, 1-9. DOI: 10.1038/s41598-017-18908-4.

Bathurst, R.G.C. (1967) Oölitic films on low energy carbonate sand grains, Bimini Lagoon, Bahamas. *Mar. Geol.,* **5**, 89-109.

Bathurst, R.G.C. (1972) Carbonate sediments and their diagenesis. Elsevier, 633 pp.

Bayet-Goll, A., **Chen, J.**, **Moussavi-Harami, R.** and **Mahboubi, A.** (2015) Depositional processes of ribbon carbonates in middle Cambrian of Iran (Deh-Sufiyan Formation, central Alborz). *Facies,* **61**, 1-18.

Belkhedim, S., **Munnecke, A.**, **Benhamou, M.**, **Nemra, A.** and **Sadji, R.** (2019) Challenging asymmetric cements as indicators of vadose diagenesis: "pseudo-gravitational" cements from the lower Pliensbachian of the Traras Mountains in NW Algeria. *Facies,* **65**, 12-35.

Benedetto, J.L. and **Sánchez, T.M.** (1972) Coelodus toncoensis nov. sp. (pisces, Holostei, Pycnodontiformes) de la Formación Yacoraite (Cretácico Superior) de la Provincia de Salta. *Ameghiniana,* **9**, 59-71.

Berg, G. (1944) Vergleichende Petrographie oolithischer Eisenerze. Reichsampt f. Bodenf., Archiv für Lagerstättenforschung, Heft **76**, 128 pp.

Beukes, N.J. (1983) Ooids and oolites of the Proterophytic Boomplaas Formation, Transvaal Supergroup, Griqualand West, South Africa. In: Peryt, T.M (Ed.), Coated Grains. Springer, Berlin, 199-214.

Blott, S.J. and **Pye, K.** (2008) Particle shape: a review and new methods of characterization and classification. *Sedimentology*, **55**, 31-63.

Brehm, U., **Krumbein, W.E.** and **Palinska, K.A.** (2006) Biomicrospheres generate ooids in the laboratory. *Geomicrobiol J.,* **23**, 545–550.

Brückmann, F.E. (1721) Specimen physicum exhibens historiam naturalem oolithi seu ovariorum piscium and concharum in saxa mutatorum. Typis Salomonis Schnorrii.

Burne, R.V., **Eade, J.C.** and **Paul, J.** (2012) The Natural History of Ooliths: Franz Ernst Brückmann's treatise of 1721 and its significance for the understanding of oolites. Hallesches Jb. *Geowiss*, **35**, 93–114.

Caputo, M.P. (1995) Sedimentary architecture of Pleistocene eolian calcarenites, San Salvador Island, Bahamas. In: Curran, H.A., White, B., (Eds.), Terrestrial and shallow marine geology of the Bahamas and Bermuda. *Geol. Soc. Am. Spec. Pap.*, **300**, 63-76.

Carozzi, A.V. (1957) Contribution à l'étude des propriétés géométriques des oolithes: l'exemple du Grand Lac Salé, Utah, USA. *Bulletin de l'Institut national genevois* **58**, 3-52.

Carozzi, A.V. (1961) Distorted oolites and pseudoolites. *J. Sed. Res.,* **31**, 262-274.

Carozzi, A.V. (1962) Cerebroid oolites. Trans. Illinois State Academy of Science, **55**, 238-249.

Carozzi, A.V. (1963) Half-moon oolites. *J. Sed. Res.,* **33**, 633-645.

Carozzi, A.V. (1964) Complex ooids from Triassic lake deposit, Virginia. *Am. J. Sci.,* **262**, 231-241.

Chanda, S.K., **Bhattacharyya, A**. and **Sakar, S.** (1977) Deformation of ooids by compaction: implications for lithification. *Geol. Soc. Am. Bull.,* **88**, 1577-1585.

Chatalov, A.G. (2005) Aragonitic-calcitic ooids from Lower to Middle Triassic peritidal sediments in the Western Balkanides, Bulgaria. Neues Jahrbuch für Geologie und Paläontologie–Abhandlungen, 87-110. DOI: 10.1127/njgpa/235/2005/87.

Chidsey, T.C.Jr., **Vanden Berg, M.D.** and **Eby, D.E.** (2015) Petrography and characterization of microbial carbonates and associated facies from modern Great

Salt Lake and Uinta Basin's Eocene Green River Formation in Utah, USA In: Bosence, D.W.J., Gibbons, K.A., Le Heron, D.P., Morgan, W.A., Pritchard, T. and Vining, B.A. (eds). Microbial Carbonates in Space and Time: Implications for Global Exploration and Production. Geological Society, London, *Spec. Publ.,* **418**, 261–286.

Cloos, E. (1947) Oölite deformation in the South Mountain fold, Maryland. *Geol. Soc. Am. Bull.,* **58**, 843-918.

Conley, C.D. (1977) Origin of distorted ooliths and pisoliths. *J. Sed. Petrol.,* **47**, 554-564.

Cónsole Gonella, C., **Griffin, M.**, **Cione, A.**, **Cavalli, S.G.** and **Aceñolaza, F.G.** (2012) Paleontología de la Formación Yacoraite (Maastrichtiano-Daniano) en el ámbito de la Subcuenca de Tres Cruces, Cordillera Oriental de la provincia de Jujuy, Argentina. In XIII Reunión Argentina de Sedimentología, 45-56.

Cónsole Gonella, C., **de Valais, S.**, **Marquillas, R.A.** and **Sánchez, M.C.** (2017) The Maastrichtian–Danian Maimará tracksite (Yacoraite Formation, Salta Group), Quebrada de Humahuaca, Argentina: environments and ichnofacies implications. *Palaeogeogr. Palaeoclimatol. Palaeoecol,* **468**, 327-350.

Cox, M.R. and **Budhu, M.** (2008) A practical approach to grain shape quantification. *Eng. Geol.*, **96**, 1-16.

Davaud, E. and **Strasser, A.** (1990) Spiny ooids: Early subaerial deformation as opposed to, late burial compaction. *Geology,* **18**, 816-819.

Davaud, E. and **Girardclos, S.** (2001) Recent freshwater ooids and oncoids from western Lake Geneva (Switzerland): indications of a common organically mediated origin. *J. Sed. Res.,* **71**, 423-429.

Davies, P.J., **Bubela, B.** and **Ferguson, J.** (1978) The formation of ooids. *Sedimentology,* **25**, 703-730.

Deelman, J.C. (1978) Experimental ooids and grapestones: carbonate aggregates and their origin. *J. Sed. Petrol.,* **48**, 503-512.

Demicco, R.V. and **Hardie, L.A.** (1994) Sedimentary structures and early diagenetic features of shallow marine carbonates. *SEPM atlas series*, **1**, 265.

Deschamps, R., **Rohais, S.**, **Hamon, Y.** and **Gasparrini, M.** (2020) Dynamic of a lacustrine sedimentary system during late rifting at the Cretaceous-Paleocene

transition: Example of the Yacoraite Formation, Salta Basin, Argentina. *The Depositional Record,* **6**, 490-523.

Diaz, M.R. and **Eberli, G.P.** (2019) Decoding the mechanism of formation in marine ooids: A review. *Earth-Sci. Rev.*, **190**, 536-556.

Diaz, M.R., Eberli, G.P., **Blackwelder, P.**, **Phillips, B.** and **Swart, P.K.** (2017) Microbially mediated organomineralization in the formation of ooids. *Geology*, **45**, 771-774.

Domokos, G., **Jerolmack, D.J.**, **Sipos, A.Á.** and **Török, Á.** (2014) How river rocks round: resolving the shape-size paradox. PloS One 9, e88657.

Dott, R.H. (1983) Episodic sedimentation; how normal is average? How rare is rare? Does it matter? *J. Sed. Res.,* **53**, 5-23.

Dunham, R.J. (1962) Classification of carbonate rocks according to depositional textures. 108-121

Dunham. R.J. (1969) Vadose pisolite in the Capitan Reef (Permian), New Mexico and Texas. In: Depositional Environments in Carbonate Rocks: A Symposium, Friedman, G.M. (Ed.), *Spec. Publ. SEPM,* **14**, 182-191.

Eardley, A.J. (1938) Sediments of Great Salt Lake Utah. *AAPG Mem.,* **22**, 1305-1411.

Edgcomb, V.P., **Bernhard, J.M.**, **Beaudoin, D.**, **Pruss, S.B.**, **Welander, P.V.**, **Schubotz, F.**, **Mehay, S.**, **Gillespie A.L.** and **Summons, R.E.** (2013) Molecular indicators of microbial diversity in oolitic sands of Highborne Cay, Bahamas. *Geobiology,* **11**, 234-251.

Esteban, M. and **Pray L.C.** (1983) Pisoids and Pisolite Facies (Permian), Guadalupe Mountains, New Mexico and West Texas. In: Peryt, T.M. (Ed.), Coated Grains, Springer, 503-537.

Ferguson, J. and **Ibe, A.C.** (1982) Some aspects of the occurrence of proto-kerogen in Recent ooids. *J. Petrol. Geol.*, **4**, 267-285.

Flügel, E. (1982) Microfacies analysis in Limestones. Springer, New York, 634 pp

Flügel, E. (2004) Microfacies of Carbonate Rocks. Analysis, Interpretation and Application. Springer, Berlin, 976 pp.

Folk, R.L. and **Lynch, F.L.** (2001) Organic matter, putative nannobacteria and the formation of ooids and hardgrounds. *Sedimentology*, **48**, 215–229.

Folk, R.L. and **Ward, W.C.** (1957) Brazos River bar: a study of significance of grain size parameters. *J. Sed. Petrol.,* **27**, 3-26.

Freeman, T. (1962) Quiet water oolites from Laguna Madre, Texas. *J. Sed. Res.,* **32**, 475-483.

Freytet, P. (1973) Petrography and paleo-environment of continental carbonate deposits with particular reference to the Upper Cretaceous and Lower Eocene of Languedoc (Southern France). *Sed. Geol.,* **10**, 25-60.

Freytet, P. and **Plaziat, J.C.** (1979) Les ooides calcaires continentaux: Diversité des formes, des gisements, des modes de formation. Recherches géographiques à Strasbourg, **12**, 69-80.

Freytet, P. and **Verrecchia, E.P.** (2002) Lacustrine and palustrine carbonate petrography: an overview. *J. Paleolimnol.*, **27**, 221-237.

Galliski, M.A. and **Viramonte, J.G.** (1988) The Cretaceous paleorift in northwestern Argentina: A petrologic approach. *J. S. Am. Earth Sci.,* **1**, 329- 342.

Gasiewics, A. (1984) Eccentric ooids. Neues Jahrbuch für Geologie und Paläontologie. Monatshefte, **4**, 204-211.

Gayet, M., **Sempre, T.**, **Cappetta, H.**, **Jaillard, E.** and **Lévy, A.** (1993) La présence de fossiles marins dans le Crétacé terminal des Andes centrales et ses conséquences paléogéographiques. *Palaeogeogr. Palaeoclimatol. Palaeoecol,* **102**, 283-319.

Ginsburg, R.N. and **Hardie, L.A.** (1975) Tidal and storm deposits, northwestern Andros Island, Bahamas. In *Tidal deposits*. Springer, Berlin, Heidelberg, 201-208.

Glumac, B., **Curran, H.A.**, **Weigner, M.M.**, **Motti, S.A.** and **Pruss, S.B.** (2012) Distribution of oolitic sediment along a beach-to-offshore transect, Pigeon cay, Cat Island, Bahamas: new insights into modern ooid formation. In: Gumble, D.W. and Kindler, P., (Eds.), Proceedings of the 15th Symposium on the Geology of the Bahamas and other Carbonate Regions. Gerace Research Center, 71-81.

Gomes, J.P.B., **Bunevich, R.B.**, **Tonietto, S.N.**, **Alves, D.B.**, **Santos, J.F.** and **Whitaker, F.F.** (2020) Climatic signals in lacustrine deposits of the Upper Yacoraite Formation, Western Argentina: Evidence from clay minerals, analcime, dolomite and fibrous calcite. *Sedimentology*, **67**, 2282-2309.

Gómez Fernández, J.J. and **Fernández López, S.R.** (1994) Condensation processes in shallow platforms. *Sed. Geol.,* **92**, 147-159.

Gomez, F.J., **Kah, L.C.**, **Bartley, J.K.** and **Astini, R.A.** (2014) Microbialites in a high-altitude Andean lake: multiple controls on carbonate precipitation and lamina accretion high-altitude lacustrine microbialites. *Palaios*, **29**, 233-249.

Guimarães, S.P. (2014) Stratigraphic analysis in Maastrichtian lacustrine deposits of the Yacoraite Formation (Salta Basin-Argentina): definition and traceability of high-resolution sequences. Master thesis, Universidade Estadual Paulista, Rìo Claro, 150 pp (In Portuguese with English abstract)

Grosso, S., **López, R.**, **Vergani, G.** and **O'leary, S.** (2013) Naturally fractured carbonate reservoirs in the Caimancito Oilfield (Yacoraite Formation), Cretaceous basin of northwestern Argentina. *Rev. Asoc. Geol. Argentina*, **70**, 53-69. (In Spanish with English abstract).

Harris, P.M., **Diaz, M.R.** and **Eberli, G.P.** (2019) The Formation and Distribution of Modern Ooids on Great Bahama Bank: *Annual Review of Marine Science,* **11**, 491-516.

Heilbronner, R. and **Barrett, S.** (2014) Image Analysis in Earth Sciences. Microstructures and Textures of Earth Materials. Springer, 520 pp.

Heller, P.L., **Komar, P.D.** and **Pevear, D.R.** (1980) Transport Processes in Ooid Genesis. *J. Sed. Res.,* **50**, 943-951.

Hernández, R., **Disalvo, A.**, **Boll, A.**, **Gómez Omil, R.** and **Galli, C.** (1999) Sequence Stratigraphy of Salta Group, focusing at sub-basins Metán-Alemania, Northwest Argentine. In: Congreso Geológico Argentino. Nacional Univ. Salta, 264–284. (In Spanish with abstract in English).

Hernández, R., **Gómez Omil, R.** and **Boll, A.** (2008) Estratigrafía, tectónica y potencial petrolero del rift cretácico en la Provincia de Jujuy. In: Coira, B.and Zappettini, E., (Eds.), Geología de la Provincia de Jujuy. Congreso Geológico Argentino, 207-232.

Hunter, R.E. (1993) An eolian facies in the Ste. Genevieve Limestone of southern Indiana, in Keith, B.and Zuppann, C., (Eds.), Mississippian oolites and modern analogs: *AAPG*, Studies in Geology, **35**, 31-47.

Husinec, A. and **Read, J.F.** (2006) Transgressive oversized radial ooid facies in the Late Jurassic Adriatic Platform interior: Low-energy precipitates from highly supersaturated hypersaline waters. *Geol. Soc. Am. Bull.,* **118**, 550–556.

Illing, L.V. (1954) Bahaman calcareous sands. *AAPG Bull.*, **38**, 1-95.

Ingalls, M., **Frantz, C.M.**, **Snell, K.E.** and **Trower, E.J.** (2020) Carbonate facies-specific stable isotope data record climate, hydrology, and microbial communities in Great Salt Lake, UT. *Geobiology*, **18**, 566–593.

Kahle, C.F. (1974) Ooids from Great Salt Lake, Utah, as an analogue for the genesis and diagenesis of ooids in marine limestones. *J. Sed. Res.,* **44**, 30-39.

Kalkowsky, E. (1908) Oolith und Stromatolith im norddeutschen Buntsandstein. Zeitschrift der deutschen geologischen Gesellschaft, 68-125.

Kidwell, S.M. (1998) Time-averaging in the marine fossil record: overview of strategies and uncertainties. *Oceanographic Literature Review*, **9**, 1546-1547.

Kidwell, S.M., **Fuersich, F.T.** and **Aigner, T.** (1986) Conceptual framework for the analysis and classification of fossil concentrations. *Palaios*, 228-238.

Krumbein, W.C. (1941) Measurement and geological significance of shape and roundness of sedimentary particles". *J. Sed. Petrol.*, **11**, 64-72.

Lasemi, Y., **Jahani, D.**, **Amin-Rasouli, H.** and **Lasemi, Z.** (2012) Ancient carbonate tidalites. In *Principles of tidal sedimentology*. Springer, Dordrecht, 567-607.

Lehrmann, D.J., **Minzoni, M.**, **Li, X.**, **Yu, M.**, **Payne, J.L.**, **Kelley, B.M.** and **Enos, P.** (2012) Lower Triassic oolites of the Nanpanjiang Basin, south China: Facies architecture, giant ooids, and diagenesis-Implications for hydrocarbon reservoirs. *AAPG bulletin*, **96**, 1389-1414.

Lehrmann, D.J., **Droxler, A.W.**, **Harris, P.**, **Minzoni, M.**, **Droxler, D.A.**, **Hopson, H. H.**, **Kelleher, C.**, **Khanna, P.**, **Lehrmann, A.A.**, **Lhemann, A.**, **Mabry, G.**, **Mercado, L.**, **Proctor, J.M.**, **Singh, P.** and **Yazbek, L.** (2020) Controls on microbial and oolitic carbonate sedimentation and stratigraphic cyclicity within a mixed carbonate-siliciclastic system: Upper Cambrian Wilberns Formation, Llano Uplift, Mason County, Texas, USA. *The Depositional Record*, **6**, 276-308.

Li, F., **Yan, J.X.**, **Algeo, T.** and **Wu, X.** (2013) Paleoceanographic conditions following the end-Permian mass extinction recorded by giant ooids (Moyang, South China). *Global Planet. Change,* **105**, 102-120.

Li, F., **Yan, J.X.**, **Chen, Z.Q.**, **Ogg, J.G.**, **Tian, L.**, **Korngreen, D.**, **Liu, K.**, **Ma, Z.L.** and **Woods, A.D.** (2015) Global oolite deposits across the Permian–Triassic boundary:

a synthesis and implications for palaeoceanography immediately after the end-Permian biocrisis. *Earth Sci. Rev.,* **149**, 163–180.

Li, F., **Gong, Q.**, **Burne, R.V.**, **Tang, H.**, **Su, C.**, **Zeng, K.**, **Zhang, Y.** and **Tan, X.** (2019) Ooid factories operating under hothouse conditions in the earliest Triassic of South China. *Global Planet. Change,* **172**, 336-354.

Li, X., **Trower, E.J.**, **Lehrmann, D.J.**, **Minzoni, M.**, **Kelley, B.M.**, **Schaal, E.K.**, **Altiner, D.**, **Yu, M.** and **Payne, J.L.** (2021) Implications of giant ooids for the carbonate chemistry of Early Triassic seawater. *Geology*, **49**, 156-161.

Loreau, J.P. and **Purser B.H.** (1973) Distribution and Ultrastructure of Holocene Ooids in the Persian Gulf. In: Purser, B.H. (Ed.), The Persian Gulf: Holocene Carbonate Sedimentation and Diagenesis in a Shallow Epicontinental Sea, Springer, 279-328.

Macellari, C.E. (1988) Cretaceous paleogeography and depositional cycles of western South America. *J. S. Am. Earth Sci.,* **1**, 373-418.

Mariotti, G. and **Fagherazzi, S.** (2012) Modeling the effect of tides and waves on benthic biofilms. *J. Geophys. Res: Biogeosciences*, 117(G4).

Mariotti, G., **Pruss, S.B.**, **Summons, R.E.**, **Newman, S.A.** and **Bosak, T.** (2018) Contribution of benthic processes to the growth of ooids on a low-energy shore in Cat Island, The Bahamas. *Minerals*, **8**, 252.

Marquillas, R.A., **del Papa, C.** and **Sabino, I. F.** (2005) Sedimentary aspects and paleoenvironmental evolution of a rift basin: Salta Group (Cretaceous–Paleogene), northwestern Argentina. *Int J Earth Sci.,* **54**, 94-113.

Marquillas, R.A, **Sabino, I.**, **Sial, A.N.**, **del Papa, C.**, **Ferreira, V.**, and **Matthews, S.** (2007) Carbon and oxygen isotopes of Maastrichtian-Danian shallow marine carbonates: Yacoraite Formation, northwestern Argentina. *J. S. Am. Earth Sci.,* **23**, 304-320.

Marquillas, R.A., **Salfity, J.A.**, **Matthews, S.J.**, **Matteini, M.** and **Dantas, E.** (2011) U-Pb zircon age of the Yacoraite Formation and its significance to the Cretaceous-Tertiary boundary in the Salta Basin, Argentina. *Cz. Geol. Cntrl. Andes Ar.*, 227-246.

Mazzullo, S.J. (1977) Shrunken (geopetal) ooids; evidence of origin unrelated to carbonate-evaporite diagenesis. *J. Sed. Res.,* **47**, 392-397.

Mazzullo, S.J. and **Birdwell, B.A.** (1989) Syngenetic formation of grainstones and pisolites from fenestral carbonates in peritidal settings. *J. Sed. Res.,* **59**, 605-611.

McGuire, K.M. (2014) Comparative Sedimentology of Lake Bonneville and the Great Salt Lake. Brigham Young University.

Mei, M. and **Gao, J.** (2012) Giant Induan oolite: A case study from the Lower Triassic Daye Formation in the western Hubei Province, South China. *Geoscience Frontiers*, **3**, 843-851.

Moreno, J.A. (1970) Estratigrafía y paleogeografía del Cretácico Superior en la cuenca del noroeste argentino, con especial mención de los Subgrupos Balbuena y Santa Bárbara: *Rev. Asoc. Geol. Argentina*, **25**, 9-44.

Myrow, P.M., **Jerolmack, D.J.** and **Perron, J.T.** (2018) Bedform disequilibrium*. J. Sed. Res.,* **88**, 1096-1113.

Newell, N.D., **Purdy, E.G.** and **Imbrie, J.** (1960) Bahamian oölitic sand. *Geol. J.,* **68**, 481-497.

O' Reilly, S.S., **Mariotti, G.**, **Winter, A.R.**, **Newman, S.A.**, **Matys, E.D.**, **McDermott, F.**, **Pruss, S.B.**, **Bosak, T.**, **Summons, R.E.** and **Klepac-Ceraj, V.** (2017) Molecular biosignatures reveal common benthic microbial sources of organic matter in ooids and grapestones from Pigeon Cay, The Bahamas. *Geobiology,* **15**,112-130.

Pacton, M., **Ariztegui, D.**, **Wacey, D.**, **Kilburn, M.R.**, **Rollion-Bard, C.**, **Farah, R.** and **Vasconcelos, C.** (2012) Going nano: a new step toward understanding the processes governing freshwater ooid formation. *Geology,* **40**, 547-550.

Paradis, O.P. (2019) Great Salt Lake Ooids: Insights into Rate of Formation, Potential as Paleoenvironmental Archives, and Biogenicity (Doctoral dissertation, University of Southern California).

Paradis, O.P., **Corsetti, F.A.**, **Bardsley, A.**, **Hammond, D.E.**, **Xu, X.** and **Walker, J.C.** (2017) Radial ooids from Great Salt Lake (Utah) as paleoenvironmental archives: Insights from radiocarbon chronology and stable isotopes. *Am. Geophys. Union Publ.,* In: *AGU Fall Meeting Abstracts*, Vol. 2017, pp. EP12A-06.

Paul, J., **Peryt, T.M.** and **Burne, R.V.** (2011) Kalkowsky's stromatolites and oolites (Lower Buntsandstein, northern Germany). In: Advances in stromatolite *Geobiology*. Springer, Berlin, 13-28 pp.

Perron, J.T., **Myrow, P.M.**, **Huppert, K.L.**, **Koss, A.R. and Wickert, A.D.** (2018) Ancient record of changing flows from wave ripple defects. *Geology,* **46**, 875-878.

Peryt, T.M. and **Piatkowski, T.S.** (1977) Algal-vadose pisoliths in the Zechstein Limestone (Upper Permian) of northern Poland. *Sed. Geol.,* **19**, 275-286.

Plee, K., **Ariztegui, D.**, **Martini, R.** and **Davaud, E.** (2008) Unravelling the microbial role in ooid formation–results of an in-situ experiment in modern freshwater Lake Geneva in Switzerland. *Geobiology,* **6**, 341-350.

Poncet, J. (1984) Microfabric and origin of Cambrian carbonate Ooids-examples from the Cambrian oolite of Carteret (Northeastern Armorican Massif, France). *Sed. Geol.,* **39**, 273-280.

Pruss, S.B. and **Clemente, H.** (2011) Assessing the Role of Skeletons in Early Paleozoic Carbonate Production: Insights from Cambro-Ordovician Strata, Western Newfoundland. In Quantifying the Evolution of Early Life. Springer, Dordrecht, 161-183 pp.

Purdy, E.G. (1963) Recent calcium carbonate facies of the Great Bahama Bank. 2. Sedimentary facies. *J. Geol.*, **71**, 472-497.

Purser, B.H. (1980) Sedimentation et diagenese des carbonates neritiques recents. Editions Technip, Paris, **1**, 366 pp.

Purser B.H. and **Loreau, J.P.** (1973) Aragonitic, Supratidal Encrustations on the Trucial Coast, Persian Gulf. In: Purser, B.H. (Ed.), The Persian Gulf: Holocene Carbonate Sedimentation and Diagenesis in a Shallow Epicontinental Sea, Springer, 342-376.

Rankey, E.C. and **Reeder, S.L.** (2011) Holocene oolitic marine sand complexes of the Bahamas. *J. Sed. Res.,* **81**, 97–117.

Rankey, E.C. and **Reeder, S.L.** (2012) Tidal sands of the Bahamian archipelago. In Principles of tidal sedimentology. Springer, Dordrecht, 537-565.

Rankey. E.C., **Riegl, B.M.** and **Steffen, K.** (2006) Form, function, and feedbacks in a tidally dominated ooid shoal, Bahamas*. Sedimentology,* **53**,191–210.

Rankey, E.C., **Goodner, H.** and **Doveton, J.** (2018) Depositional Architecture and Petrophysical Variability of an Oolitic Tidal Sand Shoal: Pennsylvanian (Missourian), Kansas, U.S.A. *J. Sed. Res*., **88**, 1114-1131.

Rasband, W.S. (2004) ImageJ. National Institutes of Health, Bethesda, Maryland, USA. Available at: http://rsb.info.nih.gov/ij/.

Risacher, F. and **Eugster, H.P.** (1979) Holocene pisoliths and encrustations associated with spring-fed surface pools, Pastos Grandes, Bolivia. *Sedimentology,* **26**, 253-270.

Roos, P.C. and **Blondeaux, P.** (2001) Sand ripples under sea waves. Part 4. *J. Fluid. Mech.*, **447**, 227-246.

Rouchy, J. M., **Camoin, G.**, **Casanova, J.** and **Deconinck, J. F.** (1993) The central palaeo-Andean basin of Bolivia (Potosi area) during the Late Cretaceous and early Tertiary: reconstruction of ancient saline lakes using sedimentological, paleoecological and stable isotope records. *Palaeogeogr. Palaeoclimatol. Palaeoecol*, **105**, 179-198.

Salfity, J.A. and **Marquillas, R.A.** (1994) Relaciones estratigráficas regionales de la Formación Yacoraite (Cretácico Superior), norte de la Argentina. Congreso Geologico Chileno, **1**, 479-483.

Sandberg, P.A. (1975) New interpretation of Great Salt Lake ooids and of ancient non-skeletal carbonate mineralogy. *Sedimentology*, **22**, 497-537.

Schindelin, J., **Arganda-Carreras, I.** and **Frise, E.** (2012) Fiji: an open-source platform for biological-image analysis. *Nature methods*, **9**, 676-682.

Sempere, T. (1995) Phanerozoic evolution of Bolivia and adjacent regions. Second ISAG, Oxford, 21 -23.

Sempere, T., **Acosta, H.** and **Carlotto, V.** (2004) Estratigrafía del Mesozoico y Paleógeno al norte del Lago Titicaca. *Spec. Publ. SGP WS*, 81-103.

Sempere, T., **Butler, R.F.**, **Richards, D.R.**, **Marshall, L.G.**, **Sharp, W.** and **Swisher III, C.C.** (1997) Stratigraphy and chronology of Upper Cretaceous–lower Paleogene strata in Bolivia and northwest Argentina. *Geol. Soc. Am. Bull.,* **109**, 709-727.

Siahi, M., **Hofmann, A.**, **Master, S.**, **Mueller, C.** and **Gerdes, A.** (2017) Carbonate ooids of the Mesoarchaean Pongola Supergroup, South Africa. *Geobiology*, **15**, 750-766.

Siesser, W.G. (1973) Diagenetically formed ooids and intraclasts in South African calcretes. *Sedimentology,* 20, 539-551.

Simone, L. (1981) Ooids: A review. *Earth Sci. Rev.,* **16**, 319-355.

Sipos, A.A., **Domokos, G.** and **Jerolmack, D.J.** (2018) Shape evolution of ooids: a geometric model: *Scientific Reports*, **8**, 1758.

Smith, L. (2019) Fitted-Fabric Grainstones-Commonly Overlooked Evidence for Vadose Diagenesis and Subaerial Exposure. *Sed. Red.,* **17**, 4-9.

Smith, B.P., **Ingalls, M.**, **Trower, E.J.**, **Lingappa, U.F.**, **Present, T.M.**, **Magyar, J.S.** and **Fischer W.W.** (2020) Physical controls on carbonate intraclasts: Modern flat pebbles from Great Salt Lake, Utah. *J. Geophys. Res: Earth Surface*, **125**, e2020JF005733. https:// doi.org/10.1029/2020JF005733

Sochan, A., **Zieliński, P.** and **Bieganowski, A.** (2015) Selection of shape parameters that differentiate sand grains, based on the automatic analysis of two-dimensional images. *Sed. Geol.,* **327**, 14-20.

Strasser, A. (1986) Ooids in Purbeck limestones (lowermost Cretaceous) of the Swiss and French Jura. *Sedimentology*, **33**, 711-727.

Summons, R.E., **Bird, L.R.**, **Gillespie, A.L.**, **Pruss, S.B.**, **Roberts, M.** and **Sessions, A.L.** (2013) Lipid biomarkers in ooids from different locations and ages: evidence for a common bacterial flora. *Geobiology,* **11**, 420-436.

Sumner, D.Y. and **Grotzinger, J.P.** (1993) Numerical modeling of ooid size and the problem of Neoproterozoic giant ooids: *J. Sed. Petrol.*, **63**, 974–982.

Taft, W.H., **Arrington, F.**, **Haimovitz, A.**, **MacDonald, C.** and **Woolheater, C.** (1968) Lithification of modern marine carbonate sediments at Yellow Bank, Bahamas. *Bull. Mar. Sci.,* **18**, 762-828.

Tasistro-Hart, A., **Maloof, A.**, **Schoene, B.** and **Eddy, M.P.** (2020) Astronomically forced hydrology of the Late Cretaceous sub-tropical Potosí Basin, Bolivia. *Geol. Soc. Am. Bull.,* 22 pp.

Trower, E.J. (2020) The enigma of Neoproterozoic giant ooids—Fingerprints of extreme climate? *Geophys. Res. Lett.,* **47**, e2019GL086146.

Trower, E.J. and **Grotzinger, J.P.** (2010) Sedimentology, diagenesis, and stratigraphic occurrence of giant ooids in the Ediacaran Rainstorm Member, Johnnie Formation, Death Valley region, California. *Precambrian Res.,* **180**, 113-124.

Trower, E.J., **Lamb, M.P.** and **Fischer, W.W.** (2017) Experimental evidence that ooid size reflects a dynamic equilibrium between rapid precipitation and abrasion rates: *Earth Planet. Sci. Lett.,* **468**, 112-118.

Trower, E.J., **Bridgers, S.L.**, **Lamb, M.P.** and **Fischer, W.W.** (2020) Ooid cortical stratigraphy reveals common histories of individual co-occurring sedimentary grains. *J. Geoph. Res. Earth Sur.,* 19 pp.

Trower, E.J., **Cantine, M.D.**, **Gomes, M.L.**, **Grotzinger, J.P.**, **Knoll, A.H.**, **Lamb M.P.**, **Lingappa, U.**, **O' Reilly, S.S.**, **Present, T.M.**, **Stein, N.**, **Strauss, J.S.** and **Fischer, W.W.** (2018) Active ooid growth driven by sediment transport in a high-energy shoal, little Ambergris cay, Turks and Caicos Islands. *J. Sed. Res.,* **88**, 1132-1151.

Tucker, M.E. and **Wright, V.P.** (1990) Carbonate Sedimentology. Blackwell, Oxford, 482 pp.

Van Ee, N.J., **Wanless, H.R.**, **Morgan, W.A.** and **Harris, P.M.** (2008) Ooids and grapestone-A significant source of mud on Caicos platform. Developing Models and Analogs for Isolated Carbonate Platforms-Holocene and Pleistocene Carbonates of Caicos Platform, British West Indies, 121-125.

Wilkinson, B.H. and **Landing, E.** (1978) "Eggshell diagenesis" and primary radial fabric in calcite ooids. *J. Sed. Res.,* **48**, 1129-1138.

Wilkinson, B.H., **Owen, R.M.** and **Carroll, A.R.** (1984) Submarine hydrothermal weathering, global eustasy, and carbonate polymorphism in Phanerozoic marine oolites. *J. Sed. Petrol.,* **55**, 171-183.

Winland, H.D. and **Matthews, R.K.** (1974) Origin and significance of grapestone, Bahama Islands. *J. Sed. Res.,* **44**, 921-927.

FIGURES AND TABLE CAPTIONS

Figure 1: Sketch showing characterization of ooid distinct attributes considered for description and counting. Red arrows indicate lining tendencies discussed in the text.

Figure 2: (A) Regional location of the study area in north-western Argentina. (B) Map Salta Group basin showing main structural highs and sub-basins, Salfity & Marquillas (1994). (C) Geological map and geographical location study area showing the outcrops of the Espinazo del Diablo section (red box) located west of Humahuaca in the Jujuy Province, Argentina.

Figure 3: Sedimentary column of the Yacoraite Formation in the study area showing (A) sedimentological details in the Lower Member (B) the ooid-rich strata within this interval. The vertical distribution of the main oolitic lithotypes studied is also shown.

Figure 4: (A) Panoramic view to the north-west of the Espinazo del Diablo range with outcrops of the complete Balbuena Subgroup (Lecho and Yacoraite formations, Late Campanian–Early Palaeocene) and overlying shales of the Maíz Gordo Formation. Outcrop thickness *ca* 500 m. (B) Sharp boundary between the aeolian complex (note the large-scale cross-bedding) of the Lecho Formation and the overlying lower member of the Yacoraite Formation. Boundary is a sharp erosive surface that can be traced throughout the complete Tres Cruces sub-basin. Distinct ridges within the lower half of Yacoraite Formation are oolite beds.

Figure 5: Outcrop photographs showing sedimentological features of a variety of oolitic-rich grainstones and rudstones, lower member Yacoraite Formation, Espinazo del Diablo section. (A) Thin-bedded wavy-flaser peloidal-oolitic grainstones. (B) Graded skeletal–oolitic packstone–grainstone. Note the low-angle cross-stratification. (C) Graded intraclastic–oolitic grainstone-rudstone with inset showing a variety of ooids, gradations and an intraclast (i, layered oolitic grainstones). (D) Cross-bedded oolitic packstone-grainstone (hammer for scale). (E) and (F) Thin-bedded mixed heterolithic lithotype showing brecciation and mud-cracks in plan view.

Figure 6: Flow-chart for thin section ooid characterization.

Figure 7: Histogram, frequency distribution of ooids and box-plots in the different lithotypes. In the upper part, the green bars represent the variation in ooid sizes within each lithotype. In the centre, red and blue bars describe the variations in roundness and circularity, respectively, of ooids among lithotypes. In the lower part, the top and bottom of each box-plot are the 25^{th} and 75^{th} percentiles, the red line within the box is the median and the whiskers show the full range of values, with outliers marked by orange circles.

Figure 8: Thin section photomicrographs of lithotypes in the Yacoraite Formation. (A) to (C) Thin-bedded wavy peloidal–oolitic grainstone and thin-bedded mixed heterolithic bedding with subaerial exposure, (D) and (E) Graded skeletal–oolitic grainstone–packstone, (F) Cross-bedded oolitic grainstone and (G) and (H) Graded intraclastic oolitic grainstone–rudstone. (A) Well-sorted sandy grainstone with small ooids commonly superficial. (B) and (C) Sandy grainstones showing a variety of ooids and peloidal-rich intraclasts. Note the superficial compound ooid in the centre of (C) (two individuals, one of them composite. (D) and (E) Bioclastic–oolitic grainstone with common elongate rod-like ooids. Ooids show a variety of nuclei: ostracods, bivalves, peloids and detrital extraclasts. Note the shell stacking and micritization in (E). (F) Well sorting and variety of ooids. (G) Poor sorting and layered intraclasts between ooids. (H) Strong bimodality.

Figure 9: Thin section photomicrographs of graded intraclastic oolitic grainstone–rudstone (A) and cross-bedded oolitic grainstone (B) to (O). (A) Moderately sorted ooids, some with irregular shapes. Note layered intraclast at bottom and the oolite intraclast at top (arrow). (B) Poorly sorted (polymodal) mostly simple multilayered ooids including different types of nuclei. Note the cerebroid ooids at top-left and bioclast nucleus (gastropod) at bottom. (C) Multilayered ooids showing various internal features as well as different nuclei. Note the large radial-concentric ooid (top-left) with a slightly eccentric core and a festoon envelope half-way and a small compound irregular ooid (arrow). (D) Simple multilayered festoon cerebroid ooids, covered bioclasts (gastropods with partly geopetal fill). (E) Moderate to well-sorted oolitic bioclastic grainstone with abundant radial-festoon-cerebroid ooids. Note that layers develop on every bioclast. (F) Poorly-

sorted grainstone–rudstone showing a laminated large compound ooid, in turn, composed by two compound ooids (with two and three distinct individuals) surrounded by broken and regenerated types. (G) Large slightly recrystallized very irregular compound grains showing local meniscus growths in re-entrants (arrows) and uneven micrite laminae in a partly rusty dolomitized matrix. (H) Oolitic grainstone with an early phreatic fringe cement and various regenerated ooids. (I) Detail of a large simple multilayered ooid with a complex slightly eccentric nucleus and distinct growths developing festoon features at mid-way separated by a notable unconformity with the outer smoother set of layers, which are partly detached probably due to slight early compaction. (J) Large simple smooth multiple-layered ooid with a subtle slightly detached angular unconformity. (K) Compound ooid formed by two distinct simple festoon ooids. Note meniscus cement (septum-like connection between the two nuclei, towards top-left). (L) Compound ooid encompassing four simple ooids (one strongly recrystallized) preserving the shape and developing a festoon exterior. Note the clear two-stage growth development and no trend in laminae thickness. (M) Compound ooid represented by the accretion of two distinct simple ooids before the common draping envelope. (N) Simple multiple-layered ooid with irregular growths given by locally aggregated clotted micrite. Note strong change of growth pattern after micrite overgrowths. (O). Large racial-concentric simple ooid similar to (N) but adding a small quartz grain between internal and external set of laminae.

Figure 10: Diagram showing possible trajectories and various paths and processes in order to explain ooid variety and evolution within the lower member of the Yacoraite Formation. From simple superficial to multilayered ooids and into more complex and compound ooid types. Different trajectories can switch-on and switch-off certain effects and various loops may start at any time, as indicated with different colours. See text for further discussion and Table 3 for a summary.

Table 1: Calculation of statistical and shape parameters of the ooids present in the lithotypes.

Table 2: Morphotypes and diversity percentage of ooids studied with a synthetic description criterion discussed considered in the *Geological setting and stratigraphy* and *Methods* sections of the text.

Table 3: Ooid formation modes following different trajectories with constructive and destructive processes involved from quantitative and qualitative analysis (see Fig.10 and the *Lithotypes, environments and ooid diversity* section in the text).

Lithotypes	Grain size			Statical parameters			Shape parameters			
	mm		Phi scale	Standard deviation (σ)	Skewness	Kurtosis		Aspect ratio (AR)	Circularity	Roundness
Thin-bedded wavy peloidal–oolitic grainstone / Thin bedded mixed heterolithic bedding	**Min.**	0.25	1.41	0.53	0.09	0.21	**Min.**	1.00	0.49	0.64
	Max.	0.37	2.00				**Max.**	4.03	0.91	0.99
	D_{50}	0.32	1.64				**Mean.**	2.52	0.86	0.81
Graded skeletal–oolitic grainstone-packstone	**Min.**	0.23	2.12	0.58	0.06	-0.02	**Min.**	1.60	0.31	0.16
	Max.	0.89	-0.23				**Max.**	6.34	0.90	0.94
	D_{50}	0.54	0.88				**Mean.**	3.70	0.61	0.55
Graded intraclastic–oolitic grainstone-rudstone	**Min.**	0.25	-0.37	0.47	-0.77	1.12	**Min.**	1.00	0.77	0.56
	Max.	1.30	2.00				**Max.**	1.78	0.91	1.00
	D_{50}	0.49	1.03				**Mean.**	1.21	0.86	0.82
Cross-bedded oolitic grainstone	**Min.**	0.32	-1.04	0.63	-0.38	-0.45	**Min.**	1.00	0.47	0.37
	Max.	2.71	1.64				**Max.**	2.71	0.91	1.00

OOID DIVERSITY	% Rel.	OOID DESCRIPTION			LITHOTYPE	SETTING
		Distribution	Nuclei	Cortex		
Simple multiple-layered ooids	60%	The distribution of size is near symmetrical and this lithotype shows the best sorting ooids. Predominantly spheroidal shape.	Sizes range from 0.03 mm to 0.18 mm for simple ooids and 0.28 mm to 0.37 mm for compound ooids. Nuclei are formed by rounded quartz grains, micritic peloids and bioclasts (ostracods). Centred nuclei predominate in this lithotype. Compound ooids have two individuals of elongate and irregular shapes.	Thickness of varies between 0.01 to and 0.07 mm. Multiple-layered ooids with two or three layers, alternately light and dark-coloured laminae. Light-coloured laminae with radially oriented acicular crystals of calcite and dark-coloured with fine cloudy micrite, the nucleus/cortex ratio is about 1.5. Superficial ooids with radial calcite or micrite cortex. Compound ooids usually develop a superficial rim *ca* 0.02 mm thick. Smooth external cortices often incomplete and decoupled.	Thin-bedded wavy peloidal-oolitic grainstone	Agitated shallow subtidal environments
Simple superficial ooids	35%					
Compound superficial ooids Fig. 8A–C	5%					
Simple multiple-layered ooids Fig. 8D–F	100%	Positively skewed asymmetrical size distribution and moderately to well-sorted ooids. Mostly ellipsoidal (rod-like) and	Sizes range from 0.07 mm to 0.64 mm. Bioclasts are included mainly as nuclei although they are plentiful in the framework of this lithotype. Centred and	Thickness of 0.03 to 0.25 mm. Rounded types show even cortex thickness; elongated types show differential thickening trends towards the shorter axis. Multiple-layered ooids	Graded skeletal–oolitic grainstone–packstone	Subtidal accumulated between fair-weather wave base and storm-wave base.

		spheroidal shape.	eccentric nuclei formed by ostracods, gastropods, bivalve fragments, peloids and a small amount of rounded quartz grains.	include two to ten layers, radial–concentric fabric alternates with thin dark micrite laminae and the nucleus/cortex ratio is 2.5. Some ooids begin with first dark micritic laminae that surrounds a bioclastic nucleus followed by a light fibrous-radial layer. External cortices exhibit smooth and irregular surfaces. In larger ooids, the last laminae may be decoupled from the others.		
Simple multiple-layered ooids	65%	Unimodal size distribution with grain population negatively skewed. Moderately to poorly sorted ooids. Mostly spheroidal shape.	Sizes range from 0.08 mm to 0.86 mm for simple ooids and 0.8 mm to 2 mm for compound ooids. Most of them have centred nuclei. Micritic intraclasts, peloids, bioclasts (mainly ostracods), ooids, fragments of concentric ooids and rounded quartz grains. Compound ooids consist of more than two or three individuals of different shapes and sizes (including simple ooids) bonded	Thickness of 0.11 to 0.8 mm. Multilayered ooids are formed of three to ten layers alternating between light radially oriented acicular crystals of calcite, radial–concentric and thin dark micritic layers and the nucleus/cortex ratios about 2.7. The external surface is in most cases smooth, although it may show subtle embayed and irregular surface.	Graded intraclastic–oolitic grainstones–rudstones	Subtidal partly cemented hardgrounds and storm layers
Compound multiple-layered ooids Figs 8G, 8H, 9A	35%					

			by a matrix of micrite or fine-grained crystalline calcite (partly dolomicrite). Broken and regenerated ooids are represented by half-moon fragments including or excluding nuclei or alternatively yielding only concentric parts of external cortices.			
Simple multiple-layered ooids	60%	Bimodal size distribution with negatively skewed and moderately to poorly-sorted ooids. Wide variety of shapes, spheroidal and ellipsoidal.	Sizes range from 0.32 mm to 2.84 mm for simple ooids including festoon types and 0.83 mm to 3.37 mm for compound ooids. Mostly centred nuclei with sharp to slightly irregular edges. Bioclasts (gastropods, bivalves and ostracods), peloids, ooids, fragments of ooids, micritic intraclasts and quartz grains. Compound ooids include clusters of two to four of ooids, intraclasts, peloids and/or quartz grains.	Thickness of 0.2 to 1.09 mm. Multiple-layered types include between five to twenty-five layers. Radial-concentric fabric alternates with thin dark micrite laminae in concentric envelopes. Ratio between nuclei/cortex is about 1.75 but forms larger than 1 mm (*ca* 1.03–2.84 mm) with thick cortex/nucleus ratio (> 4) may develop. Wide variety of external cortices, mostly festoon–cerebroid shapes showing thick cortex with internal fan-shaped crystal bundles with fascicular optic extinction alternating with micritic bands. Fan-shaped crystals protrude as convex bulges or flat-topped, some resemble micro-	Cross-bedded oolitic grainstone	Subtidal shoals and tidal-flat channel fills
Simple superficial ooids	38%					
Compound superficial ooids Fig. 9B–O	2%					

				domal columnar features. Internally, festoon ooids vary from strongly crenulated to smooth external cortices. Fragments of concentric parts represent broken and regenerated ooids. Ooids show differential thickening trend outward and zebra-like mottling. Unconformities and internal truncations are common.		
Simple multiple-layered ooids	60%	The distribution of size variation is near symmetrical. Predominantly spheroidal shape.	Sizes range from 0.03 mm to 0.18 mm for simple ooids and 0.28 mm to 0.37 mm for compound ooids. Rounded quartz grains, micritic peloids and bioclasts (ostracods). Centred and eccentric nuclei. Compound ooids have two individuals of elongate and irregular shapes.	Thickness of 0.01 to 0.07 mm. Multiple-layered ooids with two or three layers, alternately light and dark-coloured laminae. The light-coloured laminae with radially oriented acicular crystals of calcite and the dark-coloured with fine cloudy micrite and the nucleus/cortex ratio is about 1.5. Superficial ooids with radial calcite or micrite. Smooth external cortices incomplete and uneven.	Thin-bedded mixed heterolithic bedding	Tidal flats with recurrent subaerial exposure
Simple superficial ooids	30%					
Compound superficial ooids Fig. 8A–C	5%					

OOID FORMATION STAGES	CONSTRUCTIVE PROCESSES	OOID MICROTEXTURES	DESTRUCTIVE PROCESSES	OOID MICROTEXTURES
Suspension/Transport stage Sustained, periodic and/or episodic movement and/or transport, where dynamic equilibrium between lamina accretion and abrasion can be attained (*cf.* Trower *et al.,* 2017, 2018, 2020).	Lamina accretion typically controlled by physical-chemical precipitation (if carbonate saturation is attained, $\Omega >$ 1). **(Fig. 10 stages a–c)**	Crystal growth normal to lamination. Spar-rich, smooth and even laminae formed during suspension-saltation.	Grain transport modes includes suspension, saltation and rolling. Grain-to-grain and/or grain-to-bed impacts, or friction during bedload rolling transport. Lamina smoothing, truncations and discontinuities due to mechanical abrasion, also ooid fracturing and delamination due to collisions.	Depending on the conditions, smooth and even laminae or development of internal unconformities, truncated laminae and laminae laterally thinning out. Previously formed lobated shapes can be truncated or eroded. Broken or delaminated ooids.
Benthic/marine phreatic stage *Case 1*: Resting close to the sediment–water interface with no significant transport, typically in low-energy settings (*cf.* Mariotti *et al.,* 2018)	When resting, with no significant transport (*Case 1*), largely microbiologically mediated precipitation (cf. Diaz *et al.,* 2017; Plee *et al.,* 2008, 2010; Pacton *et al.,* 2012; Summons *et al.,* 2013; O'Reilly *et al.,* 2017) and thus lamina accretion (if carbonate saturation is attained, $\Omega >$ 1). **(Fig. 10 stages c–d)**	*Case 1*: Micrite-rich uneven growth (cf. Diaz *et al.*, 2017; Plee *et al.,* 2008, 2010, Pacton *et al.,* 2012; Mariotti *et al.,* 2018, O'Reilly *et al.*, 2017). Ooids and particles binding through micrite bridges, clotted textures and localized particles clustering and lumping (trap and binding). Aggregates (grapestones), coated afterwards to become incipient compound ooids (this work).	Microboring and micritization *(Case 1)*. Dissolution by corrosive fluids (for example by degradation of organic matter trapped within laminae or by pore water organic matter remineralization). c	Pit development, micritic laminae and micritic infills within borings. Microporosity within ooids, corroded, leached laminae, cement reprecipitation.
Case 2: Resting stage within a shoal environment, affected by marine phreatic processes but with episodic/cyclical transport (*cf.* Anderson *et al.,* 2020)	Alternating resting, cementation and episodic/cyclical transport (*Case 2*). If carbonate saturation is attained ($\Omega >$ 1) chemical precipitation during shallow burial within shoals is observed (Anderson *et al.,* 2020).	*Case 2: In-situ* accretion of spar-rich translucent, radial, irregular or serrate circumgranular fringe cement (cf. Anderson *et al.,* 2020). Also festoon, lobate shapes (this study).	After short residence times (*Case 2*), exhumation, remobilization, rounding and laminae smoothing.	Smooth, even lamina produced by intermittent abrasion. Eventual compound grains formation (Anderson *et al.,* 2020)

	(Fig. 10 stages e–f)	(Fig. 10 stages g, m)

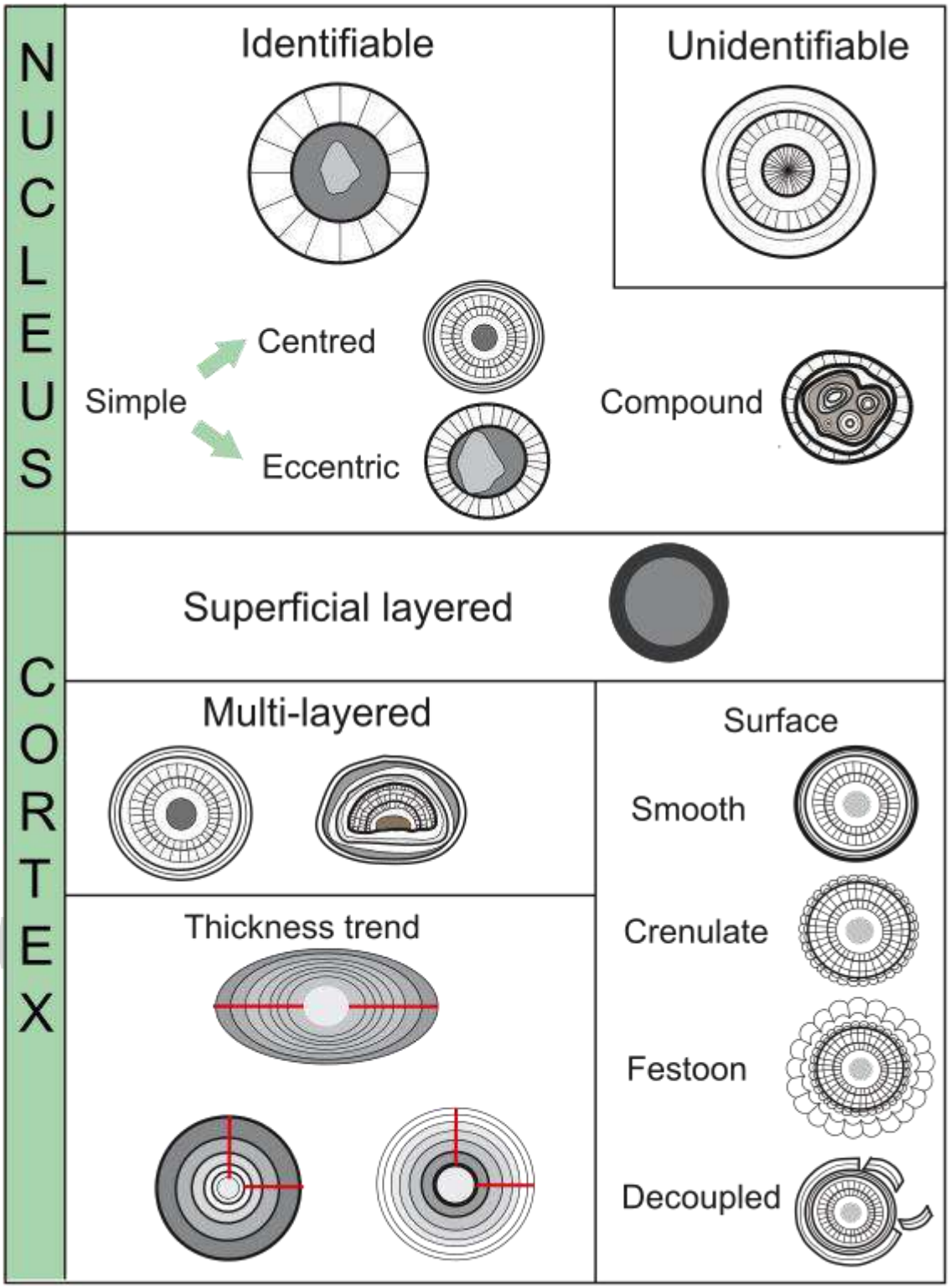

sed_13007_f1.jpg

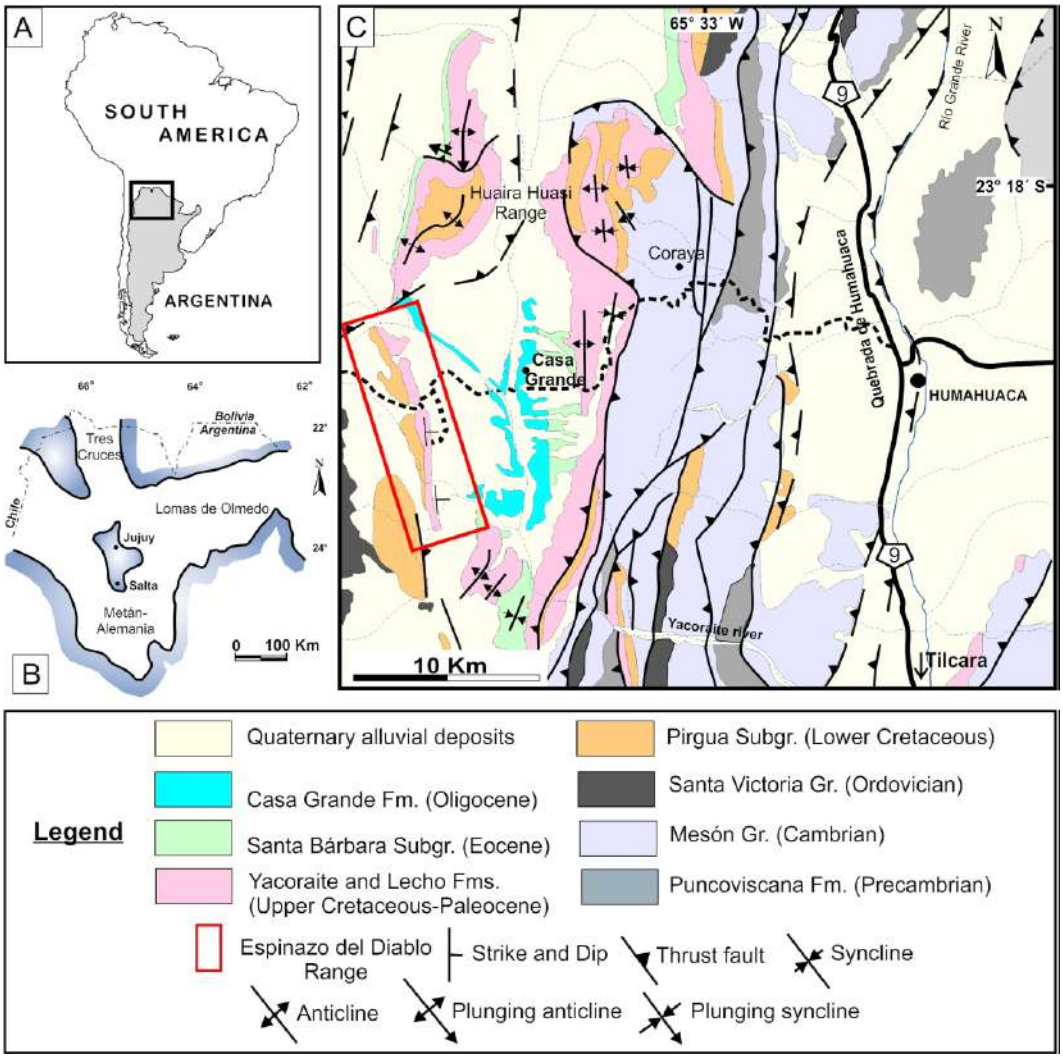

sed_13007_f2.jpg

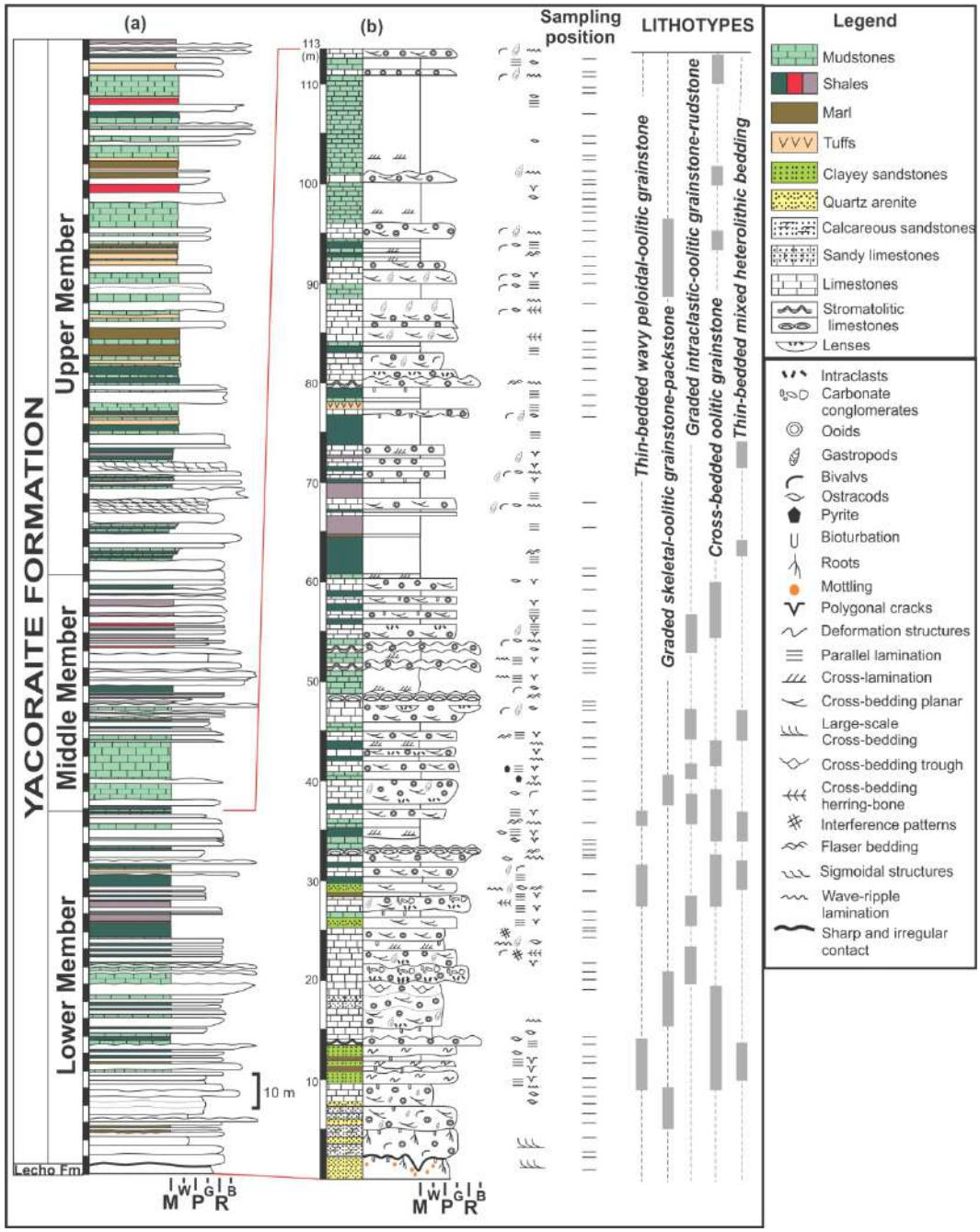

sed_13007_f3.jpg

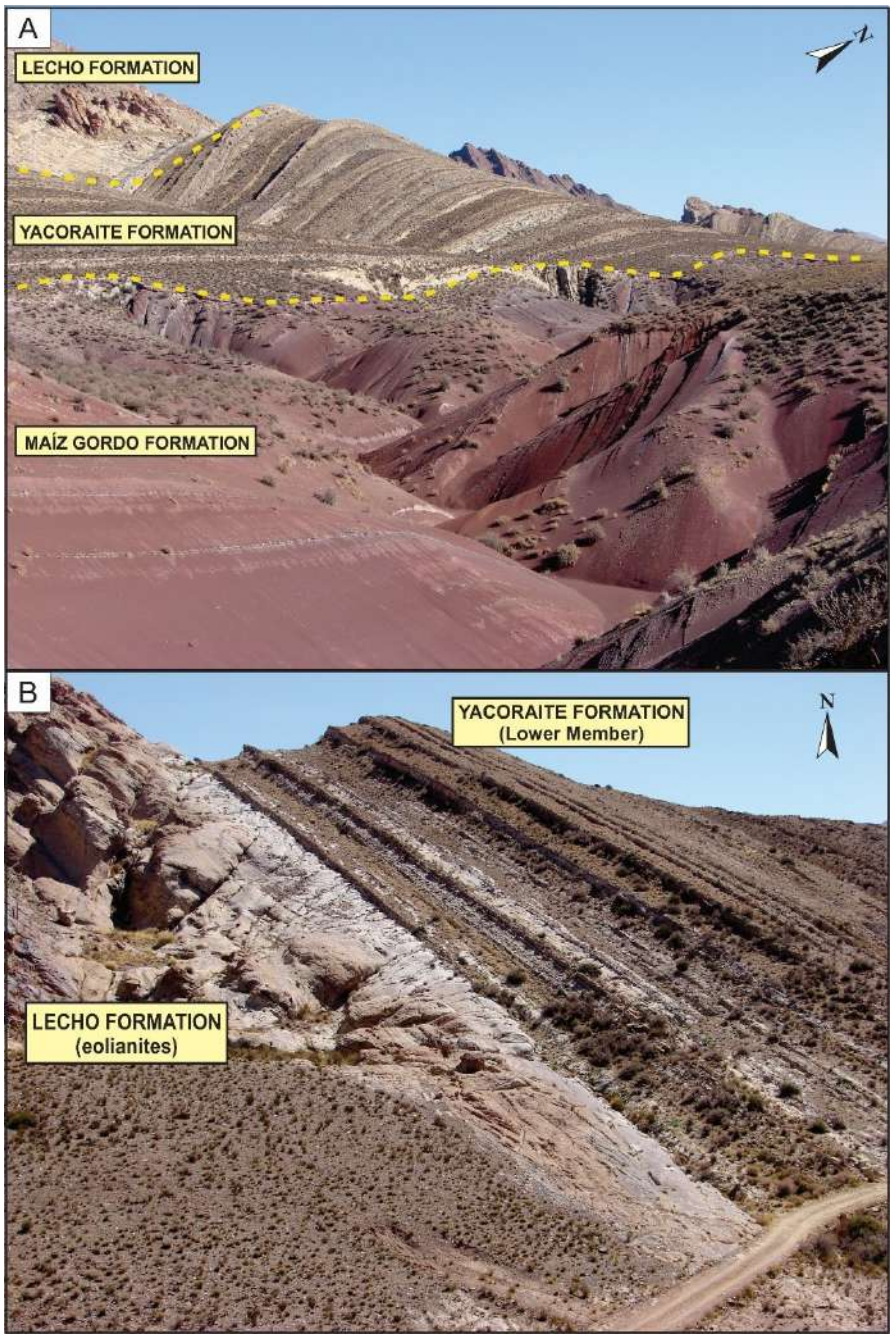

sed_13007_f4.jpg

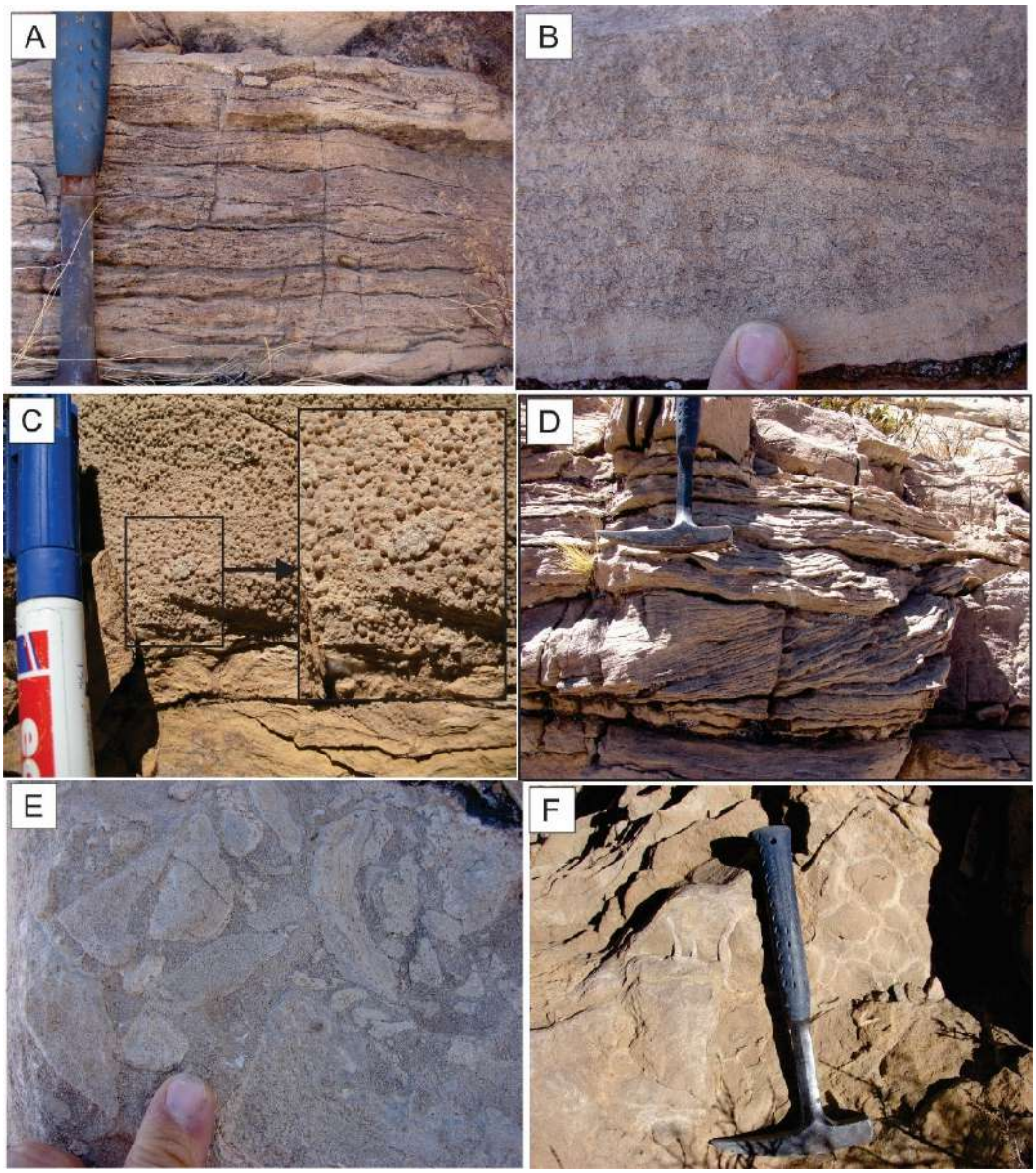

sed_13007_f5.jpg

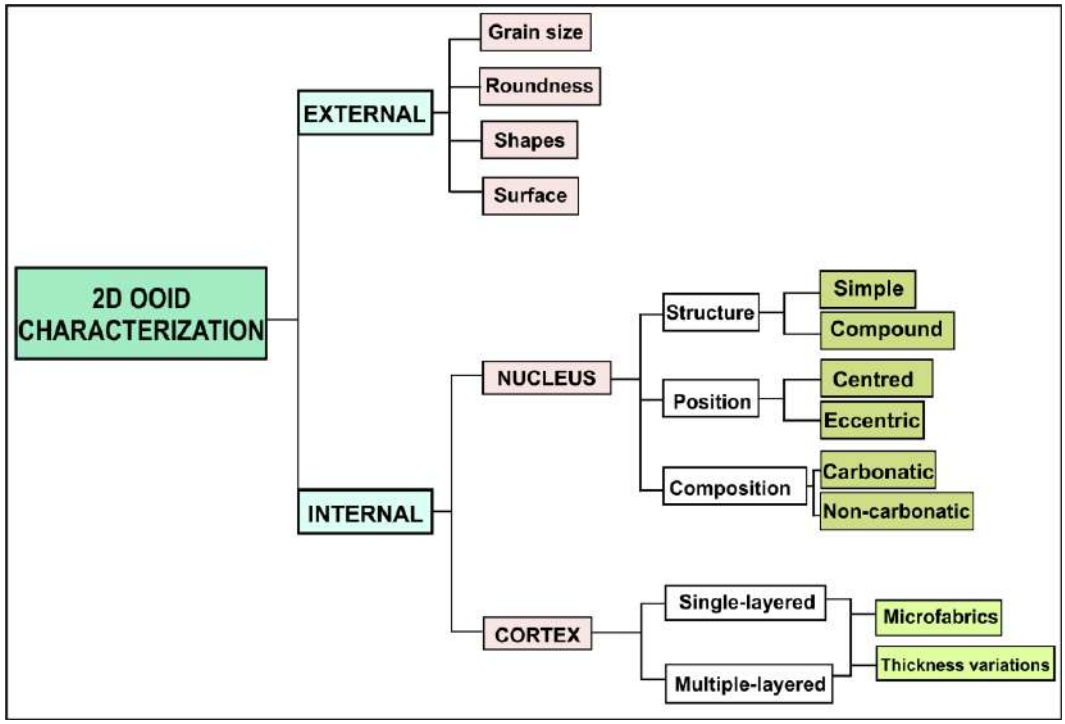

sed_13007_f6.jpg

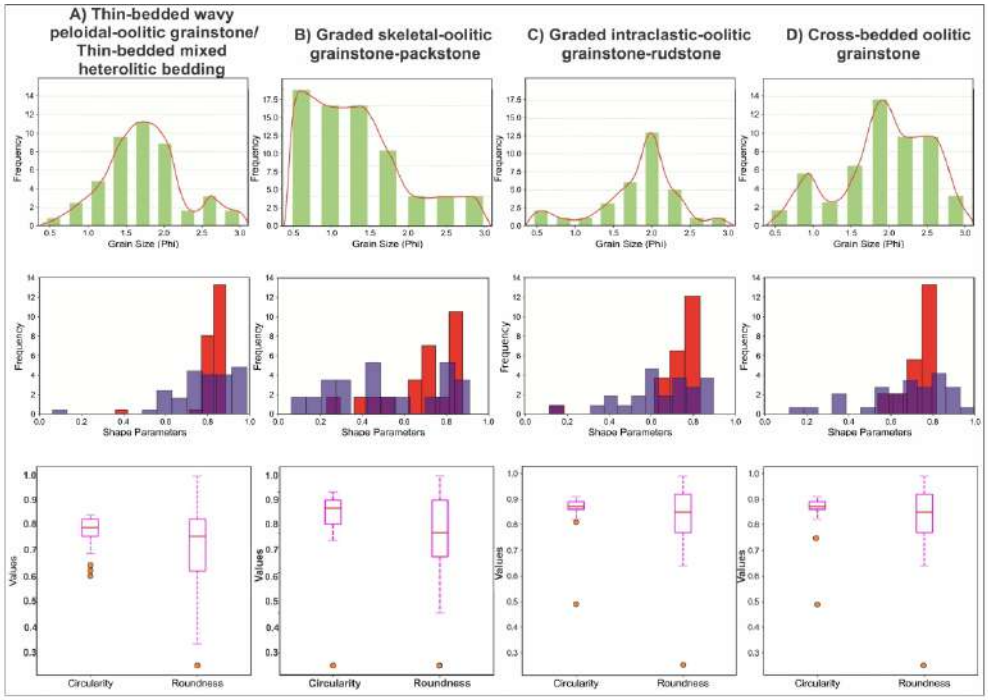

sed_13007_f7.jpg

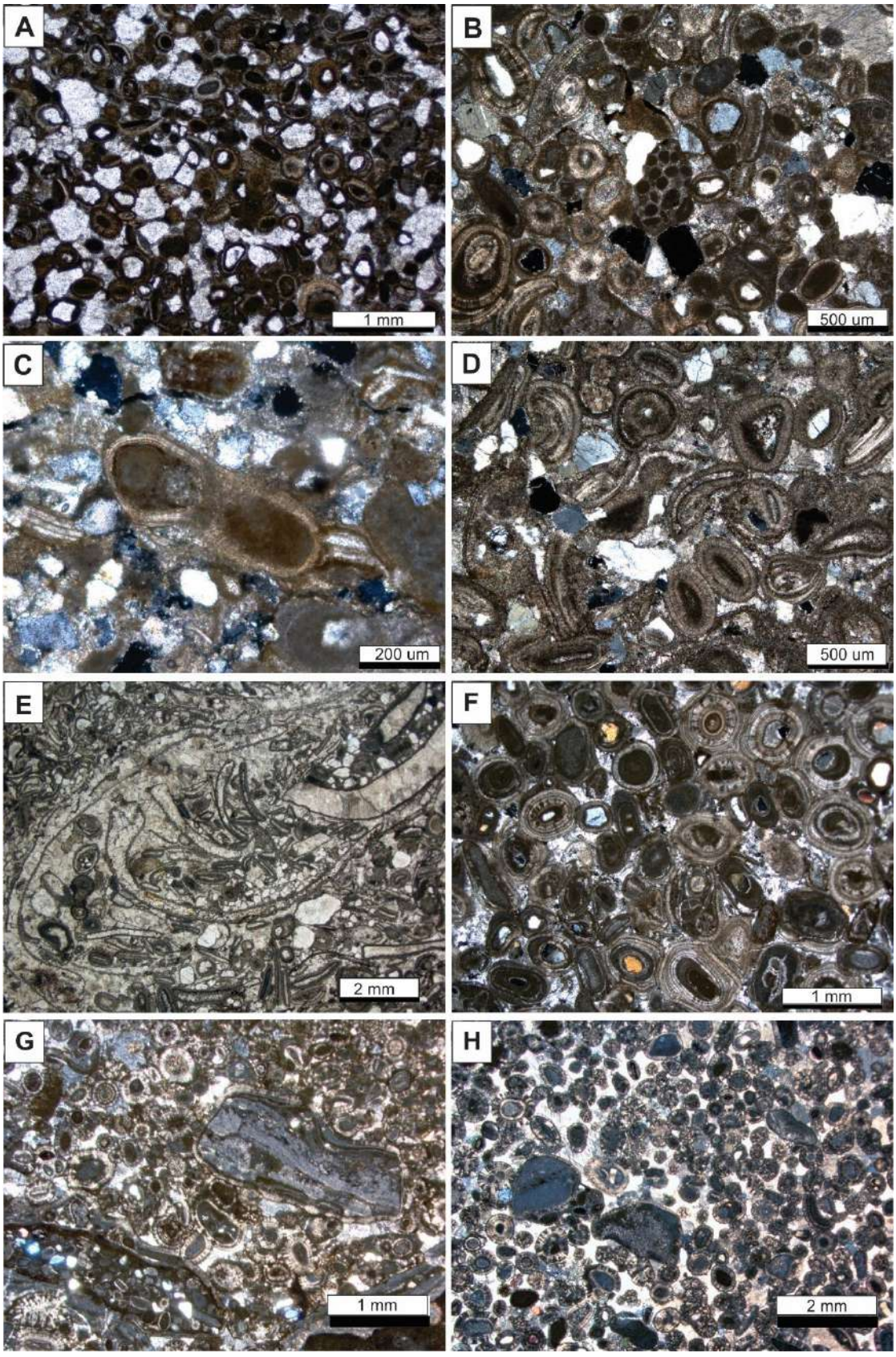

sed_13007_f8.jpg

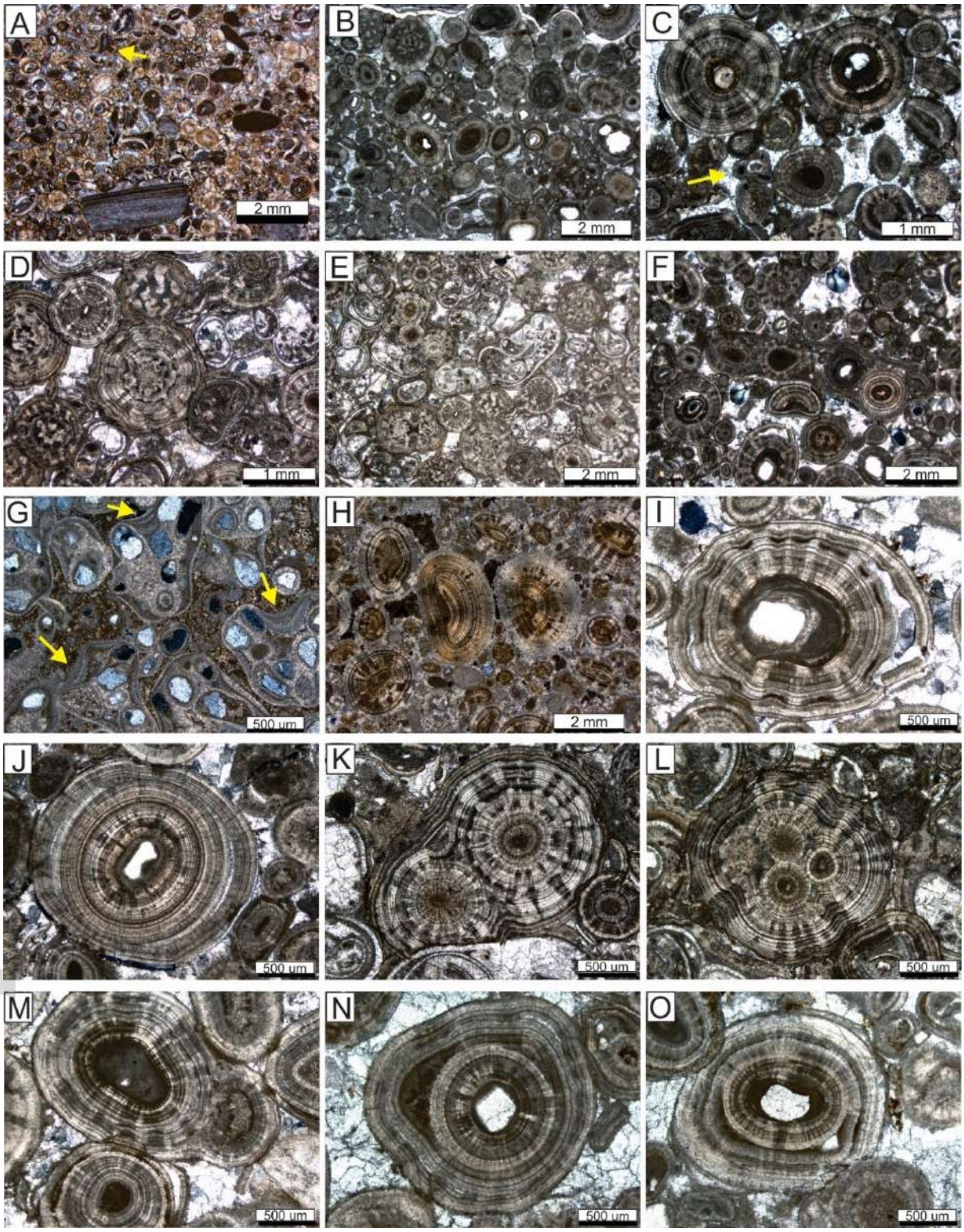

sed_13007_f9.jpg

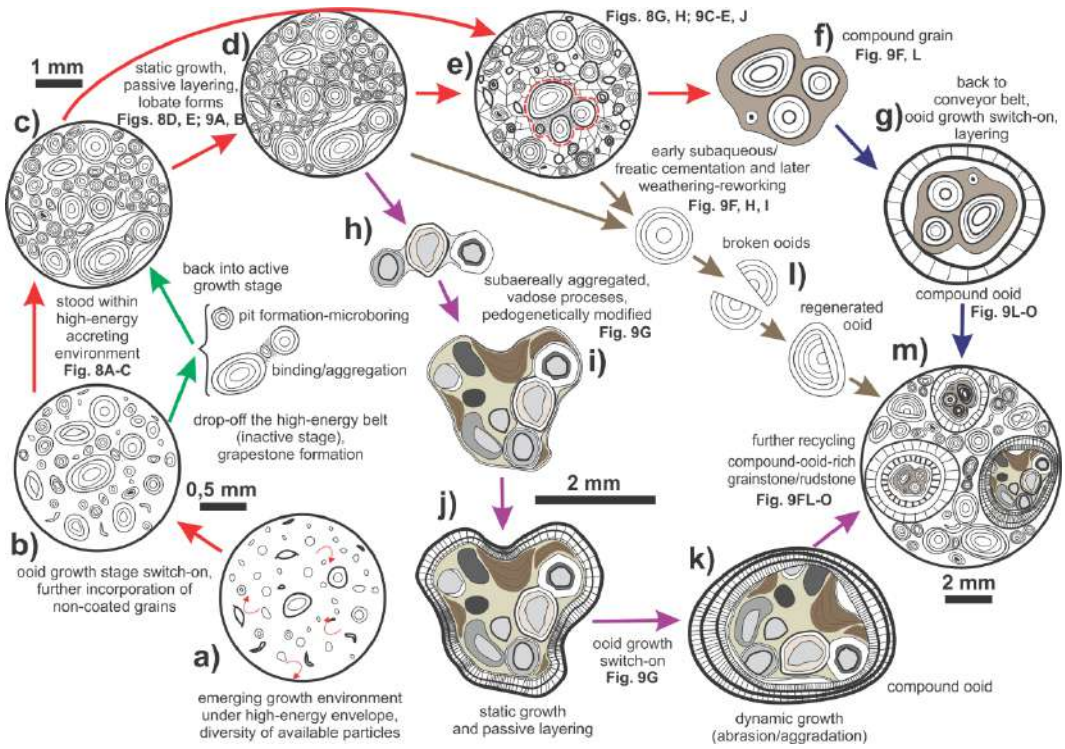

sed_13007_f10.jpg